NASA Technical Memorandum 108990

Airborne Derivation of Microburst Alerts from Ground-Based Terminal Doppler Weather Radar Information - A Flight Evaluation

David A. Hinton

August 1993

National Aeronautics and Space Administration

Langley Research Center
Hampton, Virginia 23681-0001

Summary

An element of the NASA/FAA windshear program is the integration of ground-based microburst information on the flight deck, to support airborne windshear alerting and microburst avoidance. NASA conducted a windshear flight test program in the summer of 1991 during which airborne processing of Terminal Doppler Weather Radar (TDWR) data was used to derive microburst alerts. Microburst information was extracted from TDWR, transmitted to a NASA Boeing 737 in flight via data link, and processed to estimate the windshear hazard level (F-factor) that would be experienced by the aircraft in each microburst. The microburst location and F-factor were used to derive a situation display and alerts. The situation display was successfully used to maneuver the aircraft for microburst penetrations, during which atmospheric "truth" measurements were made. A total of 19 penetrations were made of TDWR-reported microburst locations. Predicted and measured F-factors agreed well in penetrations near microburst cores. Although improvements in airborne and ground processing of the TDWR measurements would be required to support an airborne executive-level alerting protocol, the practicality of airborne utilization of TDWR data link data has been demonstrated.

Introduction

NASA and the FAA have been cooperating in a joint program since 1986 to reduce the hazard of low altitude windshear to transport category aircraft. The NASA efforts have concentrated on the airborne aspects of the problem, including the areas of microburst hazard characterization to aircraft, advanced sensor technology, and flight deck procedures and displays. The FAA has implemented ground-based solutions to the problem including training (ref. 1) and the Low-Level Windshear Alerting System (LLWAS) and the Terminal Doppler Weather Radar (TDWR) program.

In 1990 a memorandum of agreement between NASA and the FAA was signed, with a major element being the integration of ground-based windshear information on the flight deck. One purpose of the integration is to improve the timeliness of this time-critical information by providing a data link directly from the TDWR to the aircraft. Presently TDWR information is relayed verbally to aircraft by air traffic control after the aircraft has been handed off from the approach controller to the local controller. At this late stage of the approach the pilot may not receive the information until microburst contact is unavoidable (ref. 2). A second purpose of the integration is to derive microburst hazard information from the TDWR that is compatible with airborne in situ (reactive) and forward-look detection and alerting systems. Presently the TDWR system identifies the microburst phenomena by locating regions of divergence (ref. 3). The magnitude of the wind change across a microburst is measured and reported to flight crews as a wind loss to be expected and the approximate location of the threat (i.e. "expect a 50 knot loss three mile final".) Since the scale length of the wind change is not directly considered in the information sent to the crew, and the degree of hazard to an aircraft depends upon the windshear (ratio of wind change to scale length of that change, ref. 4 & 5), messages received from the ground system may conflict with data derived from onboard systems.

Ground rules were established for the integration program. These specify that 1) neither the ground systems nor current ATC/pilot roles be changed, 2) operational procedures are kept simple, 3) the air/ground roles are task tailored such that the ground system locates and classifies windshear events and the airborne system quantifies and annunciates the threat, and 4) the effort will focus on existing technology integration and evaluation. The TDWR system was to remain unchanged because years of testing have demonstrated its microburst detection capability, the system design was essentially frozen for production, and even minor changes would be prohibitively expensive. In concept, the current TDWR or integrated TDWR/LLWAS systems will remain in place and information existing within those systems will be extracted for data link to aircraft. That information will then be processed onboard along with relevant aircraft data (position, speed, altitude) to derive a situational display and hazard index for use with airborne alerting systems.

This air/ground integration concept was implemented for testing during a series of combined sensor windshear flight tests conducted by NASA during the summer of 1991 (ref. 6). These tests involved intentional microburst penetrations by the NASA Langley Boeing 737-100 equipped with experimental forward-look doppler radar and infrared windshear detection systems. A NASA Langley developed in situ algorithm (ref. 7) provided validation measurements during the microburst encounters. These flight tests were flown at two locations served by TDWR or equivalent. The first site was Orlando, Florida, which was served by the MIT Lincoln Laboratory operated TDWR testbed radar. The second site was Denver, Colorado, which was served by the National Center for Atmospheric Research (NCAR) operated Mile-High radar. This radar was functionally equivalent to the TDWR testbed and utilized the same microburst detection algorithms as the Orlando site during our flight tests. The combined sensor flight tests provided an ideal opportunity for evaluation of the air/ground information integration concept.

Nomenclature

Abbreviations:

AGL	Above ground level
ATC	Air Traffic Control
GSD	Geographic Situation Display
LLWAS	Low Level Windshear Alerting System
MIT	Massachusetts Institute of Technology
NCAR	National Center for Atmospheric Research
TDWR	Terminal Doppler Weather Radar
TSO	Technical Standard Order
UTC	Universal Coordinated Time

Symbols:

D	Aircraft aerodynamic drag.
F	Windshear hazard index, F-factor.
g	Gravitational acceleration, 9.28 m/s/s.
h	Altitude above ground.
h_r	Altitude above ground of TDWR radar beam.
H	Altitude above ground of peak microburst outflow speed.
L	Characteristic shear length for F-factor estimation.
T	Aircraft thrust.
V	Aircraft true airspeed.
Vg	Aircraft speed over the ground.
W	Aircraft weight.
Wx	Component of inertial wind along aircraft flight track.
Wh	Vertical (updraft) component of inertial wind.
β	Estimation of maximum one-kilometer wind gradient along path through microburst.
γ	Inertial flight path angle.
γ_p	Potential inertial flight path angle.
ΔR	Distance over which the TDWR-measured wind change occurs, reported by TDWR.
ΔU	TDWR-measured wind speed change through microburst.

System Concept

The baseline TDWR system (ref. 8) consists of a radar, a ground processor to identify regions of divergence and classify them as microbursts, a geographic situation display to depict microburst locations relative to runways and approach paths to the ATC tower supervisor, and an alphanumeric ribbon display

for presenting windshear and microburst information to the local controller for voice transmission to pilots (shown by non-shaded blocks in figure 1). A typical voice message from the local controller to an aircraft is "Microburst alert, threshold wind 140 at 5, expect a 50 knot loss two mile final." The concept under test required that certain data be extracted from the TDWR, automatically transmitted to an aircraft over a data link, and processed by airborne algorithms to compute the windshear hazard and provide annunciation and display. Only ground to air data link is required to provide airborne alerting. A down link may be used to provide the ATC system with information that a windshear alert has been generated by the airborne system. No changes to the existing TDWR system are required to support this concept although additional modules, depicted by the shaded blocks in figure 1, are required to transmit TDWR data to the aircraft.

The current TDWR operational concept is to detect microbursts by examining radar-observed wind velocity information for regions of divergence. When the radar detects a wind speed change of greater than 15 meters per second (29 knots), along multiple adjacent azimuth scans, over a distance of at least 1 kilometer (0.54 nm), a shape algorithm draws a microburst icon around the divergence region. "Windshear" icons are drawn around wind speed change regions of at least 7.5 meters per second. The microburst is then quantified for ATC and pilots by the wind speed change value. The actual hazard to the aircraft depends heavily, though, on the scale length of the wind speed change, i.e., the change of wind per unit distance, or shear (ref. 4 and 5). Existing airborne windshear systems as well as those under development derive an F-factor hazard index (ref. 4) that is based on wind change per unit distance and downdraft.

To provide airborne executive level alerting from TDWR information, an estimate must be made of the windshear in the microburst and the downdraft component. The information required for this estimate are readily available from the TDWR system. Since (at a readily available level) the TDWR produces a single velocity and distance number for each microburst, insufficient data are available to estimate the shear along arbitrary paths through the event. Since the microburst flow field is being characterized by a global measurement of ΔU and ΔR, the F-factor estimate becomes a "worse-case" prediction of what would be encountered while penetrating the event. The core F-factor estimate is then combined on the aircraft with TDWR microburst icon shape and location information to determine if an alert should be given. An executive level alert requires immediate corrective or compensatory action by the crew. Such a warning requires a very low nuisance alarm rate, on the order of 1 nuisance per 250 hours of system operation. A nuisance is defined as an alert received when system alert threshold conditions exist but do not produce a hazard to the aircraft. The test for validity of an executive level alert is that a threat predicted at a given time is actually experienced by the aircraft at a later time, if the pilot were to ignore the alert and continue straight ahead.

In this implementation a track-up moving map situational display depicted the microburst icons, as derived by the TDWR, the F-factor for each icon as computed onboard the aircraft, and the alerts generated from the TDWR data. The term TDWR F-factor will be used frequently in this report. This refers to the product computed on the aircraft using TDWR-supplied data. The TDWR system itself does not produce an F-factor estimate. Note that the alerts generated onboard the aircraft, using TDWR data, are not the same as the TDWR-generated alerts communicated by ATC to the aircraft. The TDWR-generated alerts are based solely on ground observations, while the airborne TDWR alerts are generated by aircraft systems using both ground-based information and aircraft specific data.

Windshear Hazard Estimation from Ground Products

The windshear hazard index used by airborne in situ detection systems and by airborne forward-look systems under development is the "F-factor" (ref. 4). The F-factor is not a description of the microburst itself, as are parameters such as wind change, reflectivity, and temperature, but is a measure of airplane performance degradation within a wind field. The F-factor scales directly with aircraft excess thrust to weight ratio so that the potential (constant airspeed) flight path angle in a windshear can be approximated

by:

$$\gamma_p = \frac{T-D}{W} - F \tag{1}$$

where T, D, and W are thrust, drag, and weight respectively. Since performance, rather than stability and control, effects are being described by the F-factor, a suitable scale length for integration of the F-factor must be chosen. Studies have shown that an appropriate scale length to be on the order of 1 kilometer (ref. 4 & 5).

From reference 4 the F-factor can be written

$$F = \frac{\dot{W}_x}{g} - \frac{W_h}{V} \tag{2}$$

where $\dot{W}_x$ is the rate of change of horizontal, along-track, wind experienced by an aircraft, Wh is updraft speed and V is aircraft airspeed. Since ground-based and airborne doppler systems cannot measure $\dot{W}_x$ or Wh directly, these parameters must be inferred from spatial wind gradients measured along the scanning beam. From reference 4, the horizontal F-factor can be determined from the spatial shear measurement by

$$\dot{W}_x = \frac{\partial W_x}{\partial x} V_g \tag{3}$$

and the updraft can be estimated from mass continuity constraints by:

$$W_h = -2h \frac{\partial W_x}{\partial x} \tag{4}$$

This leads to an F-factor estimate that can be produced from spatial measurements of windshear:

$$F = \frac{\partial W_x}{\partial x}\left[\frac{V_g}{g} + \frac{2h}{V}\right] \tag{5}$$

The windshear within a microburst can be estimated from the wind change and scale length information provided by the TDWR and an assumed wind profile. The TDWR information describes the endpoints of the peak-to-peak winds and the assumed wind profile is used to derive information about the wind field between the peaks. The horizontal wind profile of the analytical Oseguera/Bowles microburst model described in reference 9 was used to estimate the least-squares shear value over a distance L about the core of the microburst. Since aircraft performance degradation from windshear requires shear lengths on the order of 1 kilometer, or greater, a value of one kilometer for L was used in the experiment.

The TDWR microburst function is oriented towards identifying regions of divergence and characterizing those regions with a quantitative measure of wind speed change. The TDWR does this by identifying "segments" along each azimuth scan that contain a threshold wind speed change and then identifying groups of adjacent segments (ref. 3)(figure 2). Each segment is one degree apart in radar azimuth. When these groups are identified, a shape algorithm produces a racetrack or circular icon that encloses the segments yet minimizes the area of the icon. The icon is then characterized by the wind change within it. Site adaptable parameters allow tuning of the icons to isolate strong and weak wind changes in large areas of divergence and to choose how the wind change is reported (maximum segment wind change or a percentile).

For F-factor estimation from the icon data an additional parameter is required. This parameter is the distance over which the wind change is occurring and will be called ΔR. Each divergence segment has its own wind speed change and length. In this experiment the ΔU and ΔR sent to the aircraft was determined as follows. If five or fewer segments define an icon then the maximum ΔU value was sent. If this test fails, then if 20 or fewer segments define an icon send the second largest ΔU value. If more than 20 segments define an icon then send the 90th percentile segment ΔU value. In practice, nearly all icons consisted of less than 20 segments and either the largest or next largest wind speed change value was normally sent. The ΔR value was determined by examining the shear value of each segment in the icon and choosing the 85th percentile shear value. A ΔR value was then determined that would produce this 85th percentile shear when divided into the transmitted ΔU value. As an example, one icon penetrated in the 1991 flight tests (event 143) was defined by 4 segments having ΔU values of 17.1, 18.9, 22.6, and 20.2 meters/second and ΔR values of 3140, 3460, 4500, and 4210 meters, respectively. The corresponding shear values were 5.45, 5.46, 5.02, and 4.80 meters/second/kilometer. Since four segments defined the icon the largest ΔU value (22.6) was transmitted. The 85th percentile shear value was the second largest (5.45) which produced a transmitted ΔR value of 4150 meters (rounded to the nearest 10 meters). The shape tuning at Denver was slightly different but not described here due to the lack of microburst penetrations at that site.

Given the ΔU and ΔR of each icon, and the altitude of the radar measurement, a shear and downdraft estimate can be made. The resulting F-factor estimator, as originally derived by Bowles (ref. 4) is:

$$F = K\frac{\Delta U}{\Delta R}\left[\left(\frac{\Delta R}{L}\right)^2 - \left(\frac{\Delta R}{L}\right)^3 \frac{\sqrt{\pi}}{2\alpha} erf\left(\frac{\alpha L}{\Delta R}\right)\right]\left[\frac{V_g}{g} + \frac{2h_r}{V}\right] \qquad (6)$$

where K = 4.1925, α = 1.1212, h_r = the above-ground-level (AGL) altitude of the TDWR radar beam in the microburst, and L = the characteristic shear length of 1000 meters. It is this algorithm that was implemented onboard the NASA aircraft for real-time TDWR icon F-factor calculation.

Test Setup

Data Link System and TDWR Interface

To support the system concept described above it was necessary to implement a data link capability and transmit the required information. The information required to estimate the F-factor of each shape was ΔU and ΔR (to estimate shear) and the AGL altitude of the radar beam in the microburst (to estimate the downdraft contribution). Microburst icons are either circular or racetrack in shape and are described by two points and a diameter about those points (figure 2). This information was provided on the data link by transmitting the diameter and the X/Y coordinates of the two points with respect to the TDWR site. When combined on the airplane with the latitude and longitude of the TDWR site, this data enabled aircraft-relative display of the icons. Note that the diameter of a microburst shape is not necessarily the same as the ΔR of the wind change due to the various possible orientations of the racetrack icon relative to the divergence segments. In addition to ΔU, ΔR, beam altitude, and shape coordinates and diameter, the time of the TDWR measurement was transmitted for later correlation with airplane measured microburst data.

The necessary information was transmitted over the data link in the form of ASCII characters, with fixed field positions and character lengths for each parameter. Each microburst icon message was shipped in packet format, with up to eight icons described by each packet. A packet consisted of header information describing the number of icons and packets in the message, time of TDWR measurement, and a packet checksum. This header required a total of 14 ASCII characters. Each microburst icon required 25 ASCII characters. If a given message described 10 microburst icons, then two packets were required for a total of 278 ASCII characters (10 * 25 + 2 * 14). Values of microburst location were transmitted with a resolution of 100 meters, values of microburst diameter and icon size were sent with a 10 meter resolution, and wind

change was sent with a resolution of 0.1 meter per second. The radar beam altitude resolution was 10 meters.

Since the TDWR system only provides updates at approximately one-minute intervals, a low, 1200 baud rate connection provided adequate capability. A dedicated telephone line provided a connection between the TDWR and a NASA-operated data link ground station. The ground station consisted of a modem, desktop computer for monitoring the data link operation, and an MFJ Enterprises, Inc. MFJ-1270B TNC packet radio (figure 3). In addition to the end-to-end data integrity provided by the checksums, the TNC packet system also provided automatic repeat transmissions in the event a temporary radio disconnect prevented message reception. Software on the aircraft also compared the TDWR measurement time on the data link to the previous messages received, and the TDWR cockpit display continuously indicated the age of the displayed data. Warning messages were also provided on the TDWR display if the data link radio connection was lost. This data integrity checking was required since the TDWR information, in addition to its use in a research mode, was also being used in flight for real-time decisions regarding choice of microbursts to penetrate and monitoring flight safety criteria before penetration. To enhance the operational use of the TDWR data link, a waypoint type message was also implemented. This feature allowed a TDWR operator, with access to raw displays of radar reflectivity and doppler winds, to select a precise location for aircraft penetration and telemeter those coordinates to the aircraft for display. This not only assisted in finding the strongest region of a microburst icon, but also enabled the ground operators to direct the aircraft to other phenomena, such as gust fronts and developing microbursts, that did not generate icons on the data link. A waypoint type message required 16 ASCII characters and the position resolution was 100 meters.

Test Airplane and Research Flight Deck

The test aircraft was the NASA Langley Transport Systems Research Vehicle (TSRV) Boeing 737-100. this aircraft is equipped with two cockpits, a standard cockpit and a research flight deck. The research flight deck, located in the forward cabin of the aircraft, provided augmented fly-by-wire control laws and multiple electronic displays that were used for situational awareness, flight safety criteria monitoring, test progress monitoring, and flight control during setup for microburst encounters. Research flight deck displays provided precise navigation for microburst encounters near busy terminal airports.

Cockpit Situational Display and Alerting Criteria

The TDWR icon information was presented on a research flight deck moving map display, along with supporting flight state parameters, and recorded on video tape for later analysis. The supporting data (figure 4) included the TDWR data age (elapsed time since last data link reception) and in situ F-factor in the upper right corner; true airspeed, time, radar altitude and inertial wind vector in the upper left corner; ground speed and barometric altitude below the ownship symbol; and magnetic track angle above the track scale. Microburst alerts generated by the onboard TDWR algorithms were displayed by the message "TDWR ALERT" in red letters just below the track scale. The wind change and F-factor of each icon were shown numerically by labels that stepped from one icon to the next at the rate of about one icon per second (to reduce display clutter) and by color coding the icons. White was used to draw icons with F less than 0.105, amber for icons between 0.105 and 0.15 F, and red for icons with F-factors at or above 0.15. Also shown on the display were the limits of TDWR coverage and the waypoint which could be transmitted by the TDWR operator. This display is not intended to represent a format that should be implemented for fleet operational use. The display was designed for data analysis and for situational awareness and operational use during research flights.

The sketch shown by figure 4 was drawn from a video tape of the approach to event 143 on June 20, 1991. Four microburst icons are ahead of the airplane and a waypoint transmitted by the TDWR operator is on the flight path at a range of about 2.8 km (1.5 nautical miles). The aircraft has a ground speed of 122 m/s (237 knots) and the radar altimeter value is 323 m (1061 feet). A TDWR alert has been generated by

onboard logic and is displayed. The dotted line just beyond the nearest icon represents a 30 kilometer range ring from the TDWR site, which is behind the aircraft.

Three criteria were required in order to issue an executive-level alert. First, a microburst icon must exist on the projected instantaneous trajectory of the aircraft (defined by the centerline of the track-up moving map display). Second, the range from the aircraft to the icon must be less than 2.8 km (1.5 nautical miles) and, third, the icon F-factor estimate must be at least 0.105. This strategy maintains a quiet cockpit unless a microburst poses an actual threat to the aircraft, and is consistent with the candidate crew procedure described in (ref. 10). The microburst information is always presented to the pilot but no alerts are generated unless the pilot ignores the information and proceeds toward the event, or the event materializes at close range to the airplane. Note that in a classical microburst wind field the strongest wind gradient and F-factor exists in the core of the event, where the winds are weakest, while very weak wind gradients and F-factors exist in the vicinity of peak wind outflow. Since the TDWR-produced microburst shapes tend to enclose the peak-to-peak wind field, it is logical to assume that the shapes will overestimate the region of strong shear. Since insufficient data was available to determine which region within an icon contained the strongest shear, an alert was generated when any part of an icon intersected the projected flight path. The alert threshold is consistent with thresholds specified in FAA TSO-C117 (ref. 11) for the certification of reactive windshear devices and with the alert threshold for the onboard NASA in situ algorithm.

Test Procedure

The flight tests were conducted as a combined-sensor evaluation, during which the TDWR, an airborne doppler radar, and an airborne infrared sensor were tested. An airborne in situ detection algorithm developed by NASA (ref. 7) was used as a measurement standard to validate windshear predictions made with the various remote sensors. Since the nature of the experiment required microburst penetrations, a flight test technique was developed that ensured aircraft safety yet permitted meaningful measurements to be taken. The flight test procedure is presented in detail in reference 6 and aspects relevant to the TDWR experiment are summarized here.

To ensure that adequate aircraft energy reserves (altitude and airspeed) were maintained throughout each microburst penetration, limits were established for microburst strength and for entry energy conditions. The maximum microburst F-factor, as computed from the TDWR data, that could be intentionally penetrated was 0.15. The minimum aircraft energy at entry was set at 228.7 meters (750 feet) altitude AGL and 108 m/s (210 knots) airspeed or ground speed (whichever was lowest). Higher energy conditions could be flown at the discretion of the pilots, and initial microburst penetrations were typically flown at 305 to 366 meters (1000 to 1200 feet) AGL and about 118 m/s (230 knots). These limits provided a large energy margin for microburst penetrations. The aircraft was flown from the research flight deck during setup for microburst penetrations, due in part to the real-time map displays of TDWR-transmitted microburst location and waypoints, and the actual microburst penetrations were flown from the standard aircraft cockpit, due to the potential need for full control authority. Microburst penetrations were always flown in a clean (gear and flaps retracted) configuration.

Since the computed F-factor of an icon is a function of aircraft speed, and tends to increase with higher speeds, the potential existed that adding extra airspeed before a penetration may cause the computed F-factor to exceed limits. This produces the counter-intuitive situation of prohibiting a penetration at one speed and permitting a penetration at a lower speed. The higher speed is actually less hazardous since the F-factor increases approximately linearly with speed while aircraft kinetic energy increases with the square of speed, hence providing both a higher hazard index and a higher energy margin. To avoid missing acceptable penetration attempts, two TDWR displays were implemented on the TSRV research flight deck. The display used for flight safety decisions displayed computed F-factors that were based on a fixed assumed speed of 108 m/s (210 knots). The second TDWR display, video taped for research purposes, used actual aircraft speed for F-factor calculation. All TDWR and in situ F-factor values given in this paper are based on actual aircraft speed values.

For post-flight comparison of winds measured by the various sensors to the TDWR measured winds, every attempt was made to penetrate microbursts on TDWR radials either towards or away from the TDWR site. This was accomplished by defining the TDWR site as a navigation fix on the research flight deck moving map display and defining a radial from that fix through the TDWR icon being approached. This permitted precise and stable paths to be flown along the TDWR line of sight, provided other constraints such as air traffic, populated areas, or obstructions did not conflict with the desired path.

Data available from the flight tests include aircraft in situ measurements of aircraft state variables, wind components, and F-factor; logs of all data link messages transmitted to the aircraft; and video tapes of the research TDWR moving map display. Additionally, range/azimuth plots of TDWR radar reflectivity, doppler wind, and shear were provided to NASA by MIT Lincoln Laboratory. The TDWR plots portray aircraft flight path as determined by a TDWR interface to the air traffic control system, which provided radar beacon position of the airplane. The onboard NASA in situ algorithm was used as the measurement standard for evaluation of each windshear sensor. The in situ F was subjected to gust rejection filters as described in reference 7, and therefore does not resolve very short duration gusts or shears. The filter was designed in accordance with the nuisance alert and time-to-detect requirements of TSO-C117 and is approximately equivalent to a one-kilometer F-factor average at the speeds used in these flight tests. This filtering is required so that the output of the algorithm reflects windshear scales of motion that affect aircraft performance and reject scales of motion that would be perceived as turbulence.

Results

The simple data link hardware proved very reliable at both deployment locations, both while on the ground preparing for takeoff as well as while flying at low altitude 30 to 40 kilometers from the antenna site. The situation display combined with voice information from the TDWR proved invaluable for 15 to 30 minute projections of the weather situation, positioning the aircraft to intercept microbursts that were being predicted but had not yet developed, maneuvering with respect to active microbursts, and subsequent data analysis.

During the two week deployment at Orlando the NASA aircraft penetrated 19 weather events that were generating TDWR icons at the time of penetration. Numerous other events were also encountered such as gust fronts, rain shafts, and divergent flows that had not yet strengthened to the point of generating an icon or decaying microbursts that were no longer producing icons. These other events are not included in this analysis. During a three week deployment at Denver the only observed microbursts were either above flight safety reflectivity limits or could not be reached. Hence all data presented here is from the 19 icon penetrations in the Orlando area.

The data was analyzed from two perspectives. The first perspective was the overall alerting performance of the total TDWR system (TDWR, airborne processing, and alerting criteria) during the flight tests. Of particular interest was the identification of those factors affecting the accuracy of the hazard prediction. The second analysis perspective was the effect of each of the factors influencing performance. One of those factors, by necessity, is the performance of the F-factor estimation algorithm.

Overall Performance:

Table 1 summarizes the icon events encountered, icon and in situ F-factors, and whether alerts were given. Flight data is cataloged by event number here and later in this report. The date and universal coordinated time (UTC) of microburst icon entry is listed. Local time can be determined by subtracting four hours from UTC time. The TDWR F-factors given are the calculated values of the icon penetrated, taken at two times. The first value is from the most recently received data, in the aircraft flight display computers, at the time of entry into the icon. This value reflects the data shown on the moving map display at the time of entry and would be used for generating advanced warning of a microburst. The second value is from the next TDWR measurement, which more closely represents the state of the microburst while the aircraft was inside the core. The latter time data was generally measured by the TDWR while the airplane was inside

TABLE 1 - Summary of TDWR Icon Encounters

Event #	Date, 1991	Icon Entry Time, UTC	TDWR Measurement Time of Current Data on Aircraft	Measurement Age at Icon Entry, (sec)	Icon F at Entry	Next TDWR Measurement (aircraft in core)	Icon F at Next Measurement	In Situ F	TDWR Alert?	In Situ Alert?
79	6/15	19:29:14	19:28:09	65	0.11	19:29:10	0.11	0.059	Y	N
80	6/15	19:38:30	19:37:22	68	0.09	19:38:11	0.10	0.023	N	N
81	6/15	19:52:17	19:51:16	61	0.11	19:52:26	0.13	0.116	Y	Y
86	6/15	20:30:56	20:29:24	92	0.10	20:30:26	0.11	0.046	Y	N
95	6/17	18:31:49	18:31:06	43	0.19	18:32:15	0.16	0.080	Y	N
97	6/17	18:50:44	18:50:11	33	0.11	18:51:10	0.11	0.045	Y	N
106	6/18	19:10:39	19:10:01	38	0.17	19:11:11	0.17	0.042	Y	N
114	6/18	20:23:39	20:23:14	25	0.13	20:24:16	0.11	0.093	Y	N
115	6/18	20:26:03	20:25:16	47	0.10	20:26:25	no icons this update	0.048	Y	N
118	6/18	20:52:32	20:51:30	62	0.11	20:52:19	0.12	0.052	Y	N
126	6/19	17:27:47	17:26:29	78	0.15	17:27:39	0.13	0.064	Y	N
127	6/19	17:34:53	17:33:28	85	0.09	17:34:29	0.13	0.026	Y	N
133	6/19	20:31:36	20:30:12	84	0.15	20:31:15	0.17	0.100	Y	N
134	6/19	20:52:12	20:51:19	53	0.14	20:52:19	0.11	0.069	Y	N
142	6/20	20:41:34	20:40:50	44	0.09	20:41:49	0.13	0.098	Y	N
143	6/20	20:45:52	20:44:49	63	0.16	20:45:51	0.15	0.167	Y	Y
144	6/20	20:52:00	20:50:52	68	0.13	20:51:51	0.11	0.077	Y	N
145	6/20	20:57:40	20:56:52	48	0.12	20:58:02	0.11	0.060	Y	N
148	6/20	21:21:00	21:19:56	64	0.19	21:20:58	0.12	0.056	Y	N

Notes: Data in highlighted rows represent microburst core encounters.
In events 86 and 106, the TDWR data sent to the aircraft was identical from the first scan time to the second scan time, indicating a probable error.
In event 115, the microburst had decayed to a level that did not produce TDWR icons at the second measurement time. No TDWR F can be computed for this time and the previous value.
In event 148, at the time of entry another icon of F=0.11 was to the side of the 0.19 icon. This icon drifted onto the flight path between updates.

the microburst and received onboard the airplane while still in the microburst icon or shortly after exit. For example, in event 142 the aircraft entered an icon with a computed F-factor of 0.09. The radar data used for this computation was nearly a minute old, and while the aircraft was still in the icon a new data link message, containing more recently measured radar data, was received. This data produced a computed F-factor of 0.13 and generated an alert, as listed in the table. The temporal effects of the TDWR data link will be discussed in more detail below. In most microburst encounters, the TDWR system produced several small icons rather than one large icon to describe the region of shear. The TDWR icon F-factor listed describes the icon actually penetrated and not necessarily the strongest icon of the group. The in situ F-factor is the maximum value recorded during the microburst penetration. Table 2 shows the TDWR intensity data provided to the aircraft and the aircraft state variable required to calculate F-factor. This data is shown for both times listed in table 1. Also shown in table 2 is the data required for altitude correction of the icon data, which will be discussed below.

As this data shows, of the 19 icon penetrations, the airborne alerting algorithm and logic provided 18 alerts, only two of which were substantiated by an in situ alert. Figure 5 plots the peak in situ F-factor against the TDWR icon F-factor for 18 of the 19 events (one of the microbursts was not producing an icon at the latter time of table 1). The F-factor shown is the value from the TDWR data measurement taken at the latter time in tables 1 and 2, to most accurately compare in situ data to TDWR data. The data shows a strong tendency for the TDWR icon to over estimate the hazard experienced by the airplane. This performance is clearly not adequate for a system that provides executive level alerts. Further analysis is required of the factors affecting alerting performance. The primary factors affecting the performance were identified as 1) spatial offset between aircraft path and strongest windshear, 2) temporal effects from the one-minute update rate and processing and transmission delays, 3) the use of the F-factor estimation algorithm to estimate hazard from global ΔU and ΔR measurements, and 4) altitude differences between the TDWR measurement and the microburst penetration altitude of the aircraft.

Spatial Effect:

The most predominant effect was the spatial offset between flight path and hazard. As previously described, each microburst icon enclosed the entire set and length of divergence segments detected. By definition, the windshear should be very low in the vicinity of peak winds and some portion of the icons should contain little or no shear. The TDWR data available for transmission did not isolate the region of the icon that contained the shear. It is therefore possible to penetrate an icon and not encounter the full shear described by the ΔU and ΔR values. To evaluate this effect, the events were examined to determine which subset involved aircraft penetrations in or very near the microburst core.

The subset selection was done with the TDWR range/azimuth plots provided by MIT Lincoln Laboratory. The plots from the TDWR radar scans closest to the time of core penetration were used. The plots of doppler wind and shear, with aircraft track superimposed, were examined for each icon penetration. To qualify as a microburst core encounter, the plots had to show 1) that the outflow was "well defined" and 2) that the aircraft track passed in or near what could be considered the center of the outflow. "Well defined" required that the outflow take on the appearance of a microburst, rather than poorly defined decaying macrobursts (storm outflows greater than 4 km in diameter) or ragged lines of divergence. Although this selection was by necessity subjective, in many cases the plots clearly showed that the airplane flew through regions of very little shear while an area of strong shear, described by the TDWR information on the data link, was only one or two kilometers to the side. In other cases the flight path can be clearly seen passing through the strongest region of a well defined event. Figure 6 depicts a microburst core miss and figure 7 depicts a microburst core hit. Of the 19 microburst icons penetrated, only 5 (events 81, 134, 142, 143, and 144) were determined to result in microburst core penetrations. The data for those five core penetrations are outlined in tables 1 and 2, and figure 8 shows a plot of TDWR F-factor and in situ F for those events. Also shown on this plot are altitude-corrected TDWR icon values, which will be discussed later. Although insufficient data exists for statistical significance of the results, eliminating spatial offsets appears to dramatically improve the agreement between radar and in situ measurements. The average of the absolute values of the errors between the TDWR F and the in situ F was found to be 0.03 for these five events. For the entire data set of 19 events, this error value increases to 0.06.

TABLE 2 - TDWR Icon Data for each Event.

Event #	ΔU, (m/s)	ΔR, (m)	Radar Beam Altitude (m)	Aircraft Altitude at Time of Update (m)	V, (m/s)	Vg, (m/s)	Icon F	F, corrected	ΔU, corrected (m/s)
79	10 > 10	2260 > 2160	190 > 120	499 > 379	130 > 123	128 > 122	0.11 > 0.11	0.08	5.5
80	7 > 6	1590 > 1210	110 > 170	496 > 347	121 > 123	119 > 123	0.09 > 0.10	0.08	3.9
81	13 > 17	3290 > 3470	200	467 > 407	125 > 125	128 > 123	0.11 > 0.13	0.10	10.3
86	7 > 7	1790 > 1790	220	666 > 395	119 > 129	121 > 129	0.10 > 0.11	0.08	4.6
95	14 > 12	1810 > 1800	100	417 > 490	131 > 129	131 > 135	0.19 > 0.16	0.09	4.9
97	9 > 9	1950 > 1830	180	299 > 338	122 > 123	121 > 123	0.11 > 0.11	0.09	6.2
106	11 > 11	1640 > 1640	200	310 > 334	126 > 127	131 > 132	0.17 > 0.17	0.14	8.0
114	13 > 12	2390 > 2690	200	304 > 301	119 > 118	113 > 118	0.13 > 0.11	0.10	9.4
115	13 > --	3660 > ----	200	314 > 283	126 > 117	128 > 123	0.10 > --		
118	12 > 10	2110 > 1860	70 > 120	304 > 281	116 > 117	112 > 117	0.11 > 0.12	0.10	7.0
126	12 > 12	1660 > 2070	90	544 > 297	117 > 121	117 > 121	0.15 > 0.13	0.11	7.9
127	14 > 23	3740 > 3900	150 > 100	288 > 293	115 > 114	114 > 113	0.09 > 0.13	0.11	15.3
133	11 > 11	1830 > 1650	230	305 > 300	118 > 129	113 > 129	0.15 > 0.17	0.15	9.3
134	14 > 14	2610 > 3480	210 > 220	305 > 310	127 > 117	118 > 120	0.14 > 0.11	0.10	11.3
142	15 > 17	4560 > 3320	190	335 > 317	123 > 120	120 > 124	0.09 > 0.13	0.11	12.5
143	19 > 23	3020 > 4150	200	334 > 342	120 > 121	121 > 130	0.16 > 0.15	0.12	16.3
144	15 > 12	2870 > 3050	190	324 > 320	123 > 124	116 > 126	0.13 > 0.11	0.09	8.8
145	13 > 12	3070 > 2960	200 > 220	336 > 317	124 > 114	126 > 124	0.12 > 0.11	0.10	9.5
148	27 > 10	3180 > 1630	40 > 50	266 > 288	120 > 117	121 > 122	0.19 > 0.12	0.12	7.4

Notes:

Data to left of ">" is from most recent TDWR scan data on aircraft at time of icon entry. The data to the right of ">" is data from the next TDWR scan.
Notes from table 1 also apply to table 2.
The TDWR beam altitude is usually the same between the two scan times. Differing beam altitudes are generally due to changes in the radar tilt angle between 0.3 and 0.5 degrees.

Temporal Effect:

The combination of delays in data transmission and microburst growth and decay created temporal effects in the data set. Numerous delays were involved in providing microburst measurement data to the aircraft systems. The time listed for each TDWR scan is the time of the beginning of the antenna azimuth sweep, which requires 9 seconds to complete. The TDWR must then process the radar data to remove clutter returns, derive velocity, identify divergence segments, and derive microburst icons. This process requires 7 to 10 seconds. Additional delay is generated in the process of sending the required data over phone lines to the data link ground station. In the event that a waypoint type message was being transmitted by the TDWR operator, a microburst message may have to wait for transmission. The data link transmission itself will normally require on the order of one second, but any failure to complete an accurate transmission will require a repeat of the message. Temporary data link outages were observed as the aircraft maneuvered and the antenna was blocked in turns. This was typically not a problem during microburst penetrations, however, since the last three to five miles of the microburst approach was flown as straight as feasible. Finally, once onboard the aircraft, another short delay was incurred in sending the information to the display computer and drawing the new icons. From beginning of antenna sweep to display in the aircraft, the delay could easily reach 20 to 30 seconds. This delay combined with the TDWR basic update rate of once each minute could result in displayed information being up to 1.5 minutes old. Table 1 shows the age of the displayed data at the time of airplane icon entry for each event. The minimum age was 25 seconds and the oldest was 92 seconds, with an average age of 59 seconds.

In most of the events, these delays introduced little change in the icon F-factor. Table 1 shows that in three cases no F-factor change occurred between the two TDWR measurements and in five other cases the change magnitude was only 0.01. The average change magnitude was 0.02 for all events. Several events have considerable change in the two F-factors. Two cases produced changes of 0.03 F, two more produced changes of 0.04 F, and the largest change of any of the icons encountered was 0.07 F (almost 70 percent of the alert threshold). This change was not due to microburst strength changes, but rather to drift of the microburst between updates. The airplane initially entered a 0.19 F-factor icon with a weaker, 0.11 F, icon to one side. When the next TDWR update was received, while the aircraft was still in the microburst, the icons had drifted to the side and the airplane was now in a 0.12 F-factor icon. In another case (event 149 at 21:26:30 on June 20) an icon F-factor increased from 0.18 to 0.26 in one update as the aircraft was approaching for a penetration. A hard turn was made to avoid that event, which is otherwise not included in this analysis due to the lack of actual icon entry and absence of in situ data. In another case (event 115) the icons disappeared altogether in the TDWR measurement taken while the aircraft was inside the microburst icon. The alert generated in this event was not due to the primary icon listed (F=0.10), but a second, stronger, icon that the extended flight path just touched. Although changes in aircraft speed and altitude affect the computed F-factor, stable approaches to the microbursts were flown and had little influence on the F-factor computed between these two updates. For example, in the two cases where F changed 0.04 between updates, speed changes were on the order of 1 to 3 m/s. The change in F remained 0.04 when the F-factor calculations were repeated using constant speeds.

This data latency had an effect on the timing of alerts received. In three events, 86, 127, and 142, the computed icon F-factor was below the alert threshold at the time of icon entry, but exceeded the threshold and generated an alert when new data was received while still inside the icon. In one of these cases, event 86, the change in F between the two updates was only 0.01. Although all of these alerts are classified as nuisance, the in situ alert was never generated in these events, the potential exists for a valid alert to be given only after the aircraft has encountered the microburst.

F-factor Estimation Algorithm Effect:

The third factor to be examined is the performance of the F-factor estimation algorithm. For this analysis, only those five events that produced microburst core penetrations are applicable. The F-factor estimation is global to the microburst, and can only be expected to apply in an encounter with the strongest area. A primary limitation of the estimation algorithm is that it uses an assumed wind profile (ref. 9), fit to the TDWR uplink parameters, to estimate the windshear in the center of the microburst. The TDWR can

measure the radial wind component at each radar range bin and isolate regions of strong shear, but that information is not readily available as an output of the system and was not available for data link. The information that is available describes the peak outflow winds, where the shear and hazard is lowest. Therefore, the Oseguera-Bowles wind profile was used to reconstruct the shear within the core of the event, where the shear and hazard is most intense. As shown by table 1 and figure 8 , in general the TDWR F-factor agreed well with the in situ F in the core penetrations. In one event, 143, the TDWR F significantly underestimates the in situ F encountered. Figure 9 depicts, for each microburst penetration, the along-track component of the winds, as measured by the aircraft air data inertial reference system (ADIRS), and the wind profile predicted by the F-factor estimation algorithm. To produce figure 9, the TDWR ΔU data was used to establish the wind change magnitude and the TDWR ΔR value was converted to a time interval using the airplane average ground speed during the encounter. Since the in situ wind profile is biased by ambient winds, the predicted wind profile has also been biased by a constant in each plot to better compare the slopes of the two profiles. The Oseguera-Bowles wind profile does not decay as rapidly outside of the microburst as quickly as the actual winds do, but only that portion between the wind peaks is used for F-factor prediction.

In two events, 142 and 144, the in situ winds matched closely the model predicted wind. In the other events, either the TDWR wind change magnitude overestimated the in situ winds, or the scale length does not match well. Events 134 and 143 do not have the type of profile between the wind peaks that is expected by the algorithm. In event 134, the rate of wind change decreases greatly in the last half of the encounter and the scale length experienced was greater than predicted. This contributed to an over estimate of the icon F-factor. Event 143 was the only one of the five where the icon F-factor underestimated the in situ F. The wind profile within event 143 shows a large peak in the outflow in the first half of the penetration. This peak is nearly as large as the final outflow peak, which drove the TDWR estimate of ΔR. This type of wind profile may be encountered when microbursts pulse, or produce a secondary microburst surge within the expanding macroburst outflow of the initial pulse (ref. 12). In this case the TDWR may characterize the event by the larger macroburst outflow and a stronger than expected shear may be encountered by an aircraft. The TDWR system contains the information needed to resolve imbedded regions of high shear, but this information is lost in the process of characterizing an icon with a single ΔU and ΔR number. Figure 10 shows the TDWR shear plot for this encounter, as produced by MIT Lincoln Laboratory. This plot accurately locates the strong shear region in the southern side of the microburst first encountered by the airplane. The data shows that some error is inherent in estimating microburst shear from global measurements of the outflow size and strength.

Altitude Effect:

The final major factor influencing system performance was the difference in altitude between the TDWR measurement and the airplane altitude. Relatively constant F-factor with variations in altitude was used as an assumption in the TDWR F-factor implementation. As will be shown, this may be a reasonable assumption at normal takeoff and landing speeds but was not true for the research flight profiles. Although aircraft speed was used in the F-factor algorithm, the altitude of the aircraft was not included in any way. The wind change measured by the radar was used directly and the altitude of the radar beam in the microburst was used in the estimation of the vertical wind. In effect, the F-factor algorithm was assuming a penetration at the radar beam altitude. The TDWR scan elevation used for icon processing was typically 0.3 degrees above the horizon, with some scans being taken at 0.5 degrees. The altitude of the measurement varied with range from the radar site, and was typically about 200 meters in the five significant microburst penetrations. The airplane altitude during the encounters was about 300 to 400 meters.

The NASA analytical microburst models described in references 9 and 13 include a shaping function which describes the change in microburst outflow with altitude. Figure 11 depicts the function. At high altitude a microburst is predominantly a downdraft. As the wind approaches the ground the outflow speed becomes greater until surface friction effects begin to lower the outflow speed. The shaping function is based on mass continuity, boundary layer friction, and wind profiles produced by the Terminal Area Simulation System (TASS) numerical microburst model, which has been extensively validated against observed

microburst data (references 14 and 15). The shaping function p(h) provides the ratio of outflow speed to maximum outflow speed at any arbitrary altitude. Given this shaping function, the shear estimate (β) at any altitude can be expressed as the shear at the altitude of maximum outflow multiplied by p(h). The shaping function is:

$$p(h) = \frac{e^{-0.22h/H} - e^{-2.75h/H}}{0.7386} \tag{7}$$

where H is the altitude of maximum outflow speed. The shear estimate at an arbitrary altitude is described by:

$$\beta = \beta' p(h) \tag{8}$$

where β' is the shear at the altitude of maximum outflow. We can express F at any altitude as:

$$F_1 = \beta' p(h_1)\left(\frac{V_g}{g} + \frac{2h_1}{V}\right) \tag{9}$$

and

$$F_2 = \beta' p(h_2)\left(\frac{V_g}{g} + \frac{2h_2}{V}\right) \tag{10}$$

or by rearranging 9 and 10:

$$F_2 = F_1 \frac{p(h_2)\left(\frac{V_g}{g} + \frac{2h_2}{V}\right)}{p(h_1)\left(\frac{V_g}{g} + \frac{2h_1}{V}\right)} \tag{11}$$

Equation 11 was used as an altitude correction algorithm where F_1 is the uncorrected TDWR F-factor estimation, h_1 is the TDWR radar beam altitude, and h_2 is the airplane altitude. F_2 then becomes the F-factor estimate at the airplane altitude. The altitude of maximum outflow, H, was assumed to be 90 meters. Table 2 summarizes the original F and altitude-corrected F for each icon penetration. Also shown is the wind change reported by the TDWR and an altitude corrected value, used in figure 12 to compare the in situ along-track wind profiles to the predicted wind at flight altitude. Figure 8 shows the altitude-corrected icon F-factors and the peak in situ F-factors, along with the original icon F values. In each case, the altitude correction reduced the icon F-factor estimate. Examination of figures 8, 9, and 12 shows that the altitude correction generally improved the wind profile fit to the actual winds experienced, in terms of the slope between the wind peaks. The most notable exception is event 143, where the shear estimation error caused by the localized shear within the larger shear is exaggerated by the altitude correction. This effect is only coincidental, and had the aircraft been flying well below the radar beam altitude, the altitude correction may have increased the F-factor estimate and masked the wind profile effect. Application of altitude correction to the data reduced the average of the absolute values of the F-factor estimation errors to 0.04 for full set of icon penetrations, and to 0.02 for the five core penetration events.

The altitude correction just described was more significant to the data collected in the NASA flight tests than it would likely be in operational use. As the altitude of microburst penetration increases above the altitude of maximum outflow, the horizontal wind change decreases while the downdraft increases. Since the F-factor experienced by the airplane is proportional to horizontal wind gradient multiplied by ground speed and downdraft divided by airspeed, the horizontal component of F-factor tends to decrease with increasing altitude while the vertical component tends to increase with altitude. The relative magnitude of

these two changes depends on airplane speed. At normal approach speeds the change in the two components tend to be of similar magnitude. The result is that the F-factor does not vary greatly with altitude above the altitude of maximum outflow up to altitudes where microbursts no longer pose a safety threat (about 300 to 350 meters). At the high speeds used in the microburst flights, however, the total F-factor is more sensitive to the horizontal wind gradient than the downdraft, and the measured F-factor decreases more quickly with increased altitude. Table 3 shows the altitude-corrected output of the TDWR F-factor algorithm for an aircraft flying at 67, 82, and 118 m/s (130, 160, and 230 knots) at altitudes of 50, 100, 200, and 300 meters, for an assumed microburst with a ΔU of 25 m/s and ΔR of 3000 meters. The three speeds approximate normal approach speeds and the NASA microburst penetration speed. The calculations assume that the altitude of maximum outflow is 90 meters and that the radar measurement is taken at that altitude. At 67 and 82 m/s, the change in F-factor from 100 meters to 300 meters is only about 0.01, while at 118 m/s the change is nearly 0.04. Below the altitude of maximum microburst outflow both horizontal winds and vertical winds decrease, leading to reduced F-factor. Some form of altitude correction may be required even at normal approach speeds, since variations in distance between the microburst and the TDWR site may cause the radar measurement to be taken well above or below the peak outflow altitude of the microburst.

TABLE 3 - Effect of Aircraft Speed on Altitude Compensation of TDWR Icon F-factor

	Airspeed and Ground Speed (m/s)		
Aircraft Altitude (m)	67	82	118
50	0.106	0.122	0.164
100	0.137	0.151	0.192
200	0.149	0.154	0.179
300	0.144	0.143	0.156

Conclusion

This experiment demonstrated the practicality of transmitting ground-based windshear information to an aircraft via data link, processing that information on the aircraft to estimate the windshear hazard index (F-factor), then providing the information on an electronic map display for operational use. Other than extraction of the required products, no changes were made to the TDWR system for this capability, and low data rate communications were adequate. In the very limited number of microburst core penetrations made in the 1991 flight tests, the estimated F-factor compared very favorably to the peak in situ F-factor. The average absolute error between the TDWR prediction and the in situ F, with temporal, spatial, and altitude effects minimized, was 0.02 F. Considering that the two measurements are taken from different locations, at different times, and with different spatial resolution, this agreement is excellent.

When all effects are included, the performance of the prediction deteriorates significantly. The division of a microburst into multiple icons, and the size of the TDWR icons relative to the area of significant shear, contributed to the aircraft track missing the desired microburst region in 14 of 19 icon penetrations. This effect can create hazard estimation errors on the order of 100% of the alert threshold. Microburst growth and decay between the TDWR measurement updates were typically on the order of 20% of the alert threshold, with some updates producing changes of 40% of threshold. The error magnitude possible with these short latency times suggests that the timeliness of ATC verbal transmission to aircraft may be marginal in some situations. The update delay combined with a 30 second interval for transmission and display of the data on the aircraft could lead to late alerts and aircraft encounters with hazardous shears. The altitude effect observed in these encounters produced estimation errors on the order of 10 to 20% of the alert threshold. Implementation of a real-time altitude correction algorithm can easily be done on the aircraft, and was performed for additional microburst research flights in the summer of 1992.

Although the TDWR and data link system, as tested, provided high-confidence advisory information and excellent situational awareness, an excessive number of nuisance alerts would prevent the system from

being used to drive executive level cockpit alerting. These nuisance alerts were primarily due to the spatial effect of the aircraft missing the shear region altogether, and not to any inability to measure the shear from the ground. The information required to minimize this limitation is resident within the TDWR system, but not planned as an output product of production TDWR systems. More complete use of the ground system capabilities, by implementing shear-based detection algorithms and icon shapes, may greatly improve the utility of the TDWR microburst information to the end users.

More microburst penetrations with TDWR coverage are required to increase confidence in the results and show statistical significance. Research flights were conducted in 1992 at both Denver and Orlando, during which numerous microburst penetrations were made. The analysis of the 1992 data will be the subject of a future research report.

References

1. Federal Aviation Administration: Windshear Training Aid, Example Windshear Training Program, February 1987.
2. Schlickenmaier, Herbert W.: Windshear Case Study: Denver, Colorado, July 11, 1988, DOT/FAA/DS-89/19, November 1989.
3. Brislawn, Kristi; Wilson, Wesley F.; MaHoney, William; Wiener, Gerry, and Goodrich, Kent: Microburst Detection and Display by TDWR: Shape, Extent, and Alarms, Third International Conference on the Aviation Weather System, Anaheim, CA., 1989.
4. Bowles, Roland L.: Reducing Windshear Risk Through Airborne Systems Technology, Paper Presented at the 17th Congress of the International Council of the Aeronautical Sciences, Stockholm, Sweden, September 9-14, 1990.
5. Wanke, C.; and Hansman, R.J.: Alert Generation and Cockpit Presentation for an Integrated Microburst Alerting System, Paper Presented at 29th Aerospace Sciences Meeting, January 7-10, 1991, Reno, Nevada, AIAA-91-0260.
6. Lewis, Michael S.; Yenni, Kenneth R.; Verstynen, Harry A.; and Person, Lee H.: Design and Conduct of a Windshear Detection Flight Experiment, Paper Presented at the 6th AIAA Biennial Flight Test Conference, August 24-26, 1992, Hilton Head, SC., AIAA 92-4092.
7. Oseguera, Rosa M.: Bowles, Roland L.; and Robinson, Paul A.: Airborne In Situ Computation of The Wind Shear Hazard Index, Paper Presented at the 30th Aerospace Sciences Meeting & Exhibit, January 6-9, 1992, Reno, NV., AIAA 92-0291.
8. Bernella, D.M.: Terminal Doppler Weather Radar Test Bed Operation - Orlando, January - June 1990, MIT Lincoln Laboratory Project Report ATC-180, DOT/FAA/NR-91/6, November 4, 1991.
9. Oseguera, Rosa M. and Bowles, Roland L.: A Simple, Analytic 3-Dimensional Downburst Model Based on Boundary Layer Stagnation Flow, NASA TM-100632, July 1988.
10. Bowles, Roland L.; and Hinton, David A.: Windshear Detection: Airborne System Perspective, Paper Presented at the WINDSHEAR-One Day Conference, London, England, November 1, 1990.
11. Federal Aviation Administration, Airborne Windshear Warning and Escape Guidance Systems for Transport Airlines, Technical Standard Order C117, July 24, 1990.
12. Proctor, Fred: Three-Dimensional Numerical Simulation of the 20 June 1991, Orlando Microburst, published in Airborne Wind Shear Detection and Warning Systems, Fourth Combined Manufacturers' and Technologists' Conference, Williamsburg, Va, April 14-16, 1992, NASA CP-10105, DOT/FAA/RD-92/19-I
13. Vicroy, Dan D.: A Simple, Analytical, Axisymmetric Microburst Model for Down Draft Estimation, NASA TM-104053, DOT/FAA/RD-91/10, February, 1991.
14. Proctor, F. H.: The Terminal Area Simulation System, Volume 1: Theoretical Formulation, NASA CR 4046, 1987.
15. Proctor, F. H.: The Terminal Area Simulation System, Volume 2: Verification Experiments, NASA CR 4047, 1987.

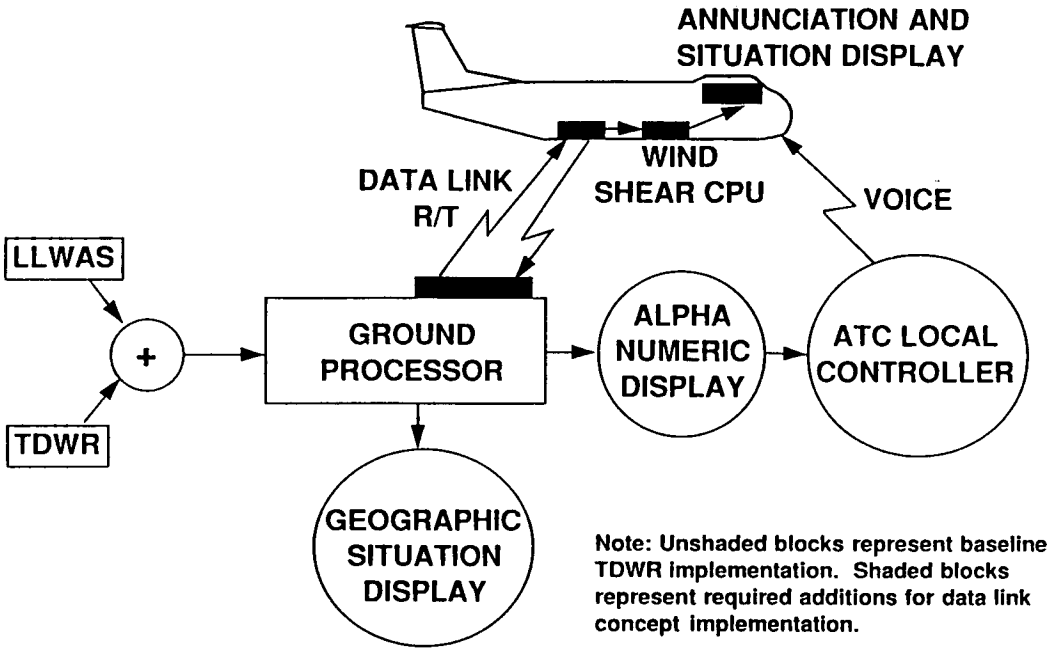

Figure 1 - TDWR System Architecture

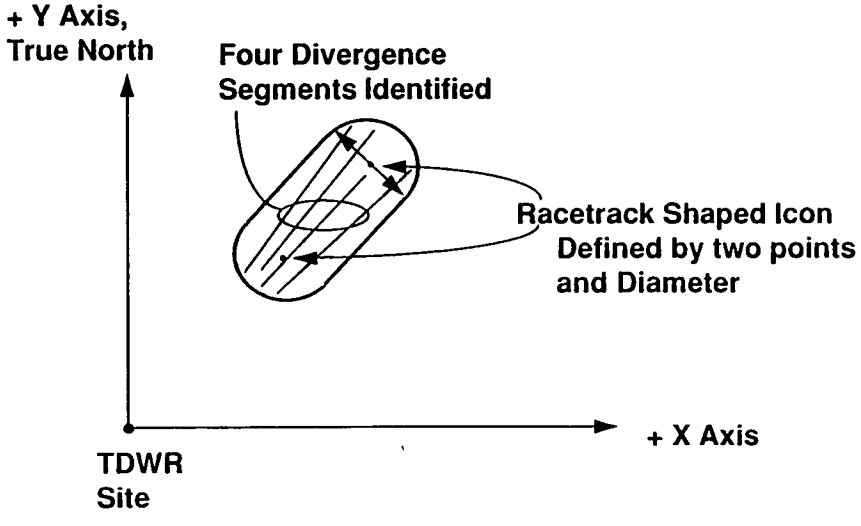

Figure 2 - TDWR Icon Shapes

Figure 3 - TDWR Data Link Ground Station

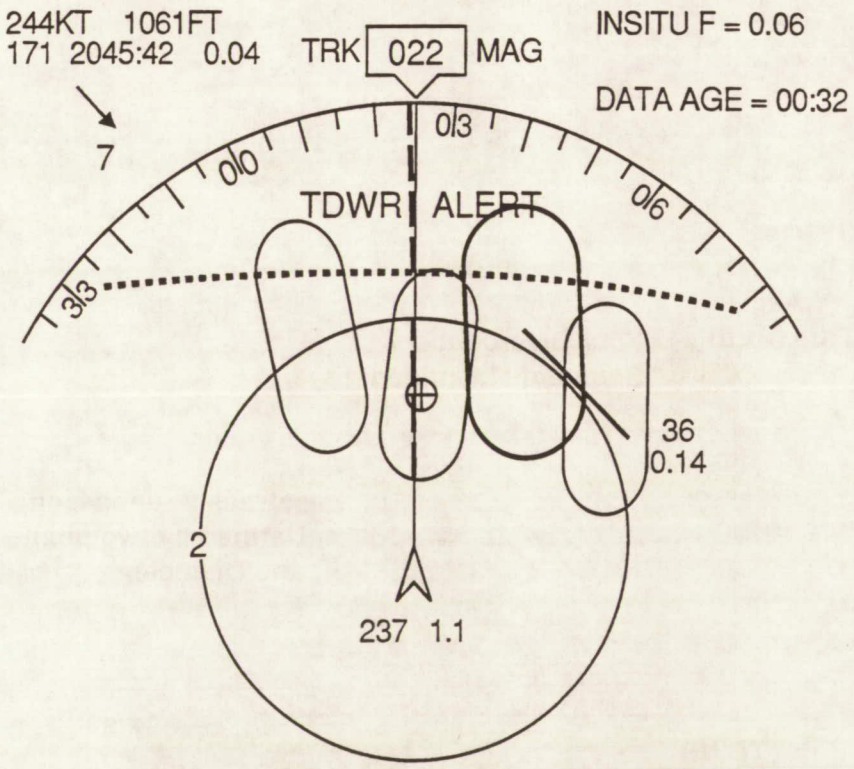

Figure 4 - TDWR Information Display on Airborne Moving Map

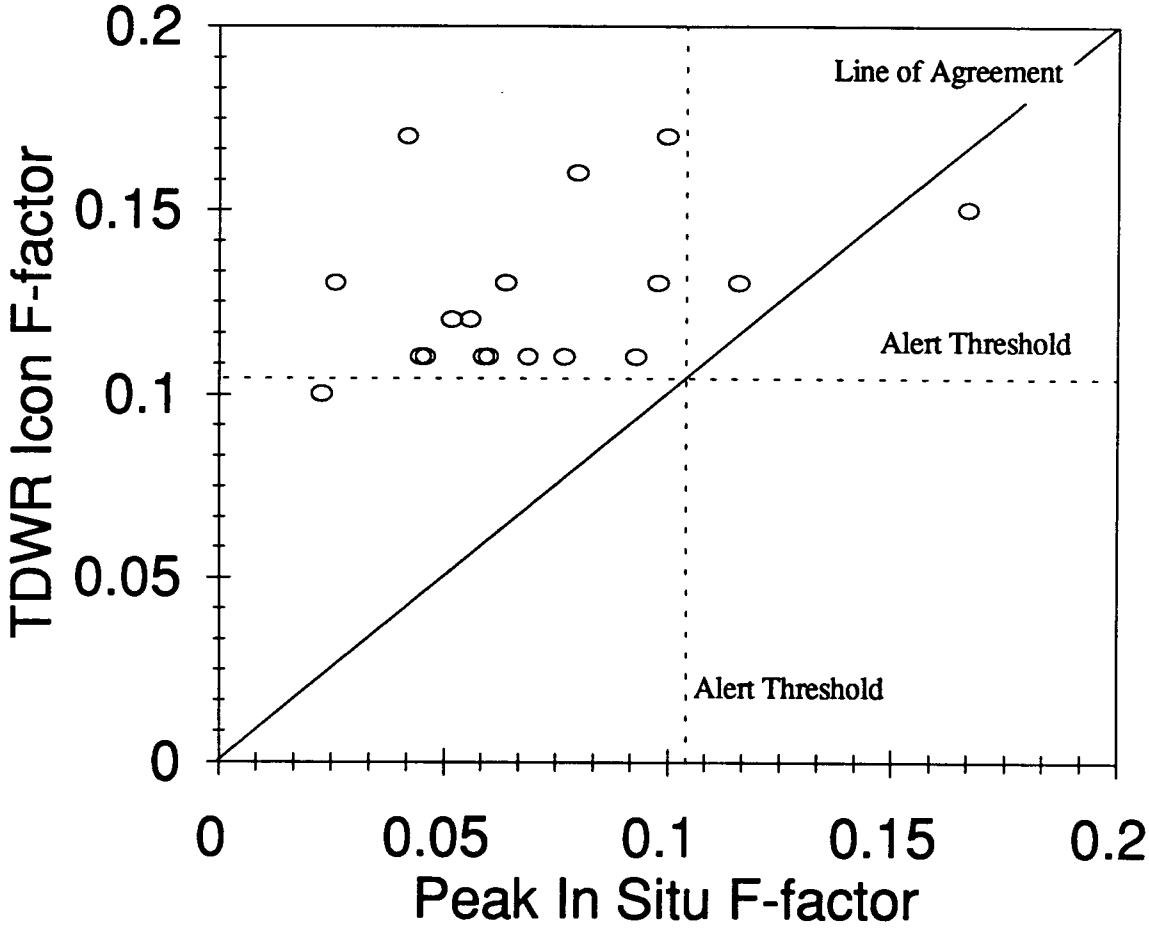

Figure 5 - Peak In Situ and TDWR F
for 18 Microburst Icon Penetrations

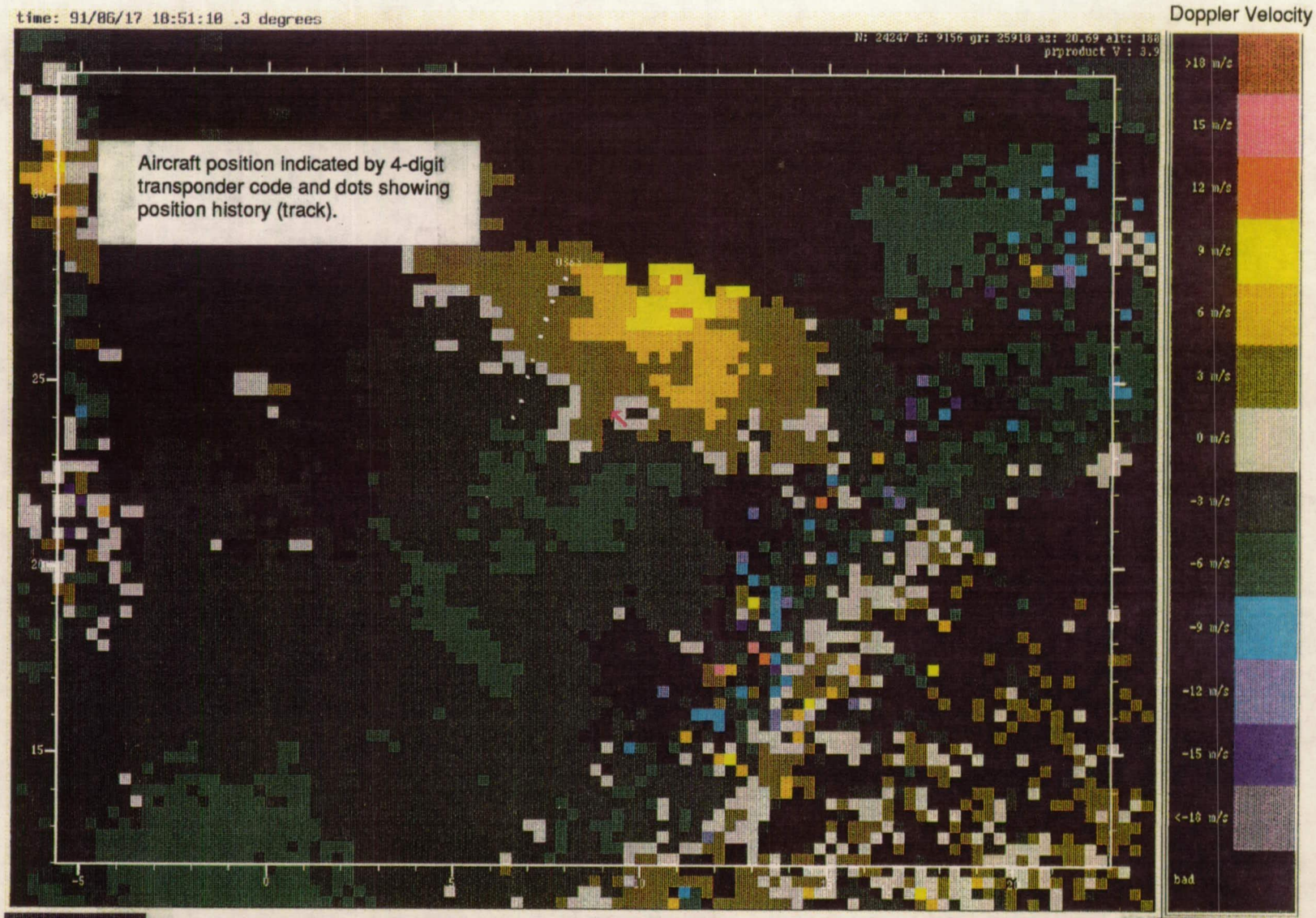

Figure 6 - Example of the Aircraft missing the Microburst Core, Event 97

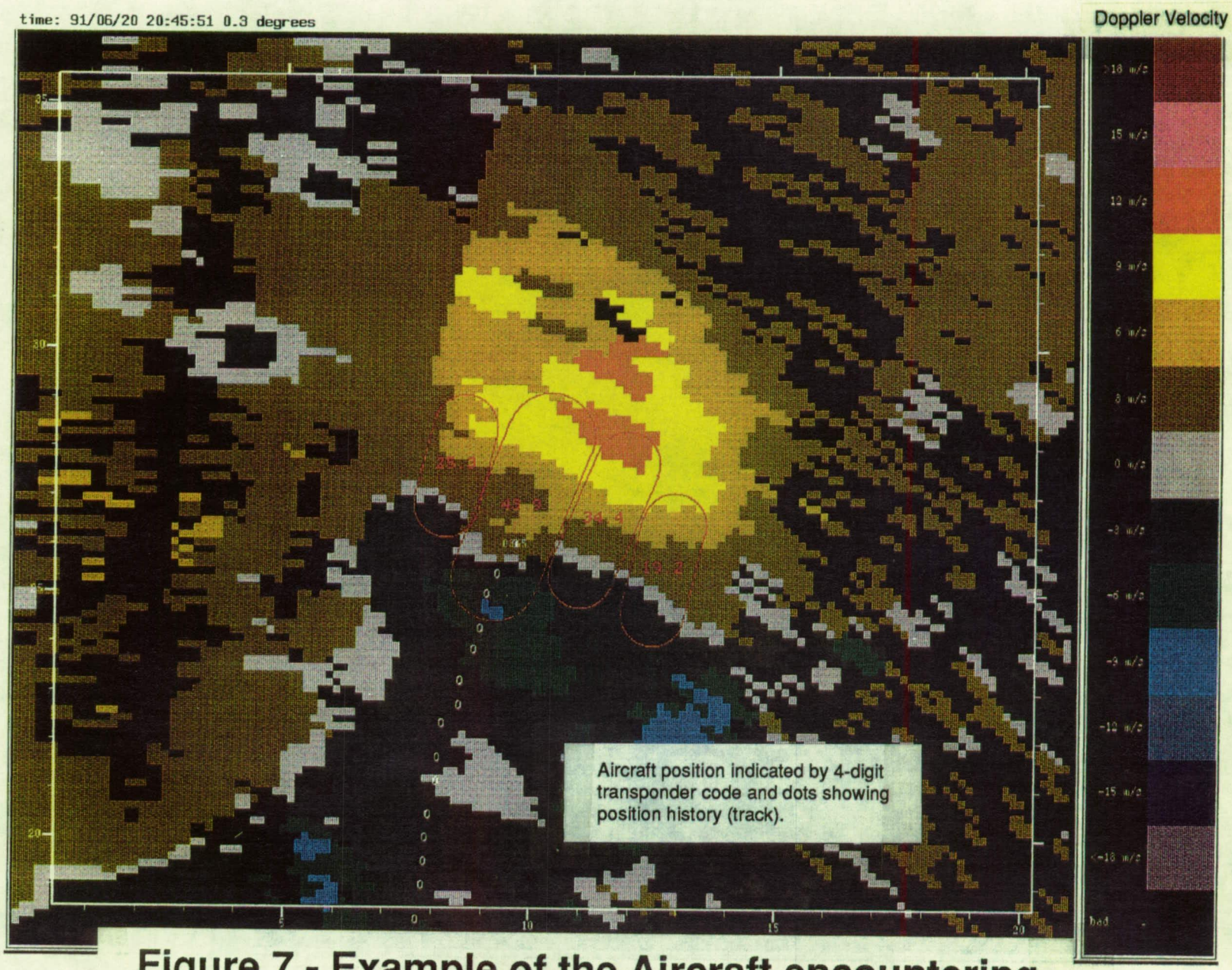

Figure 7 - Example of the Aircraft encountering the Microburst Core, Event 143

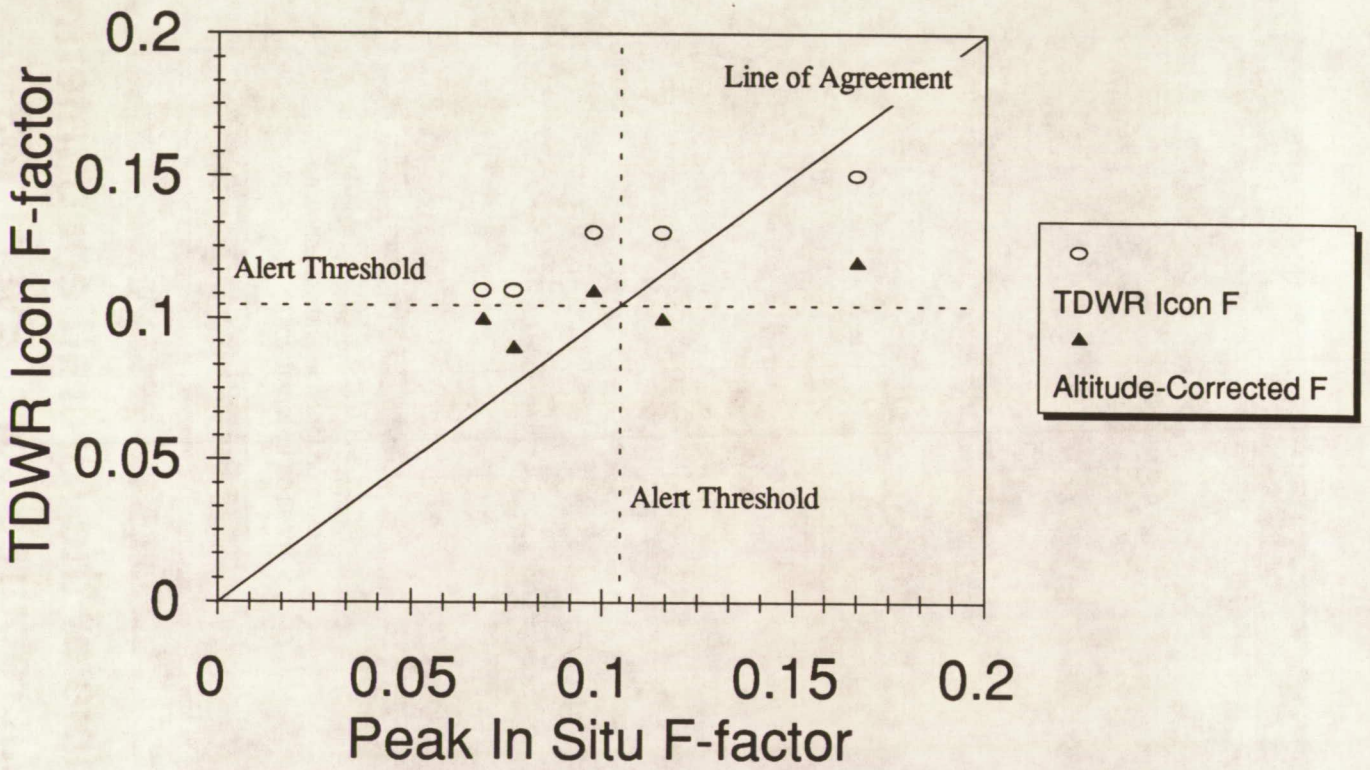

Figure 8 - Peak In Situ and TDWR F
for 5 Microburst Core Penetrations

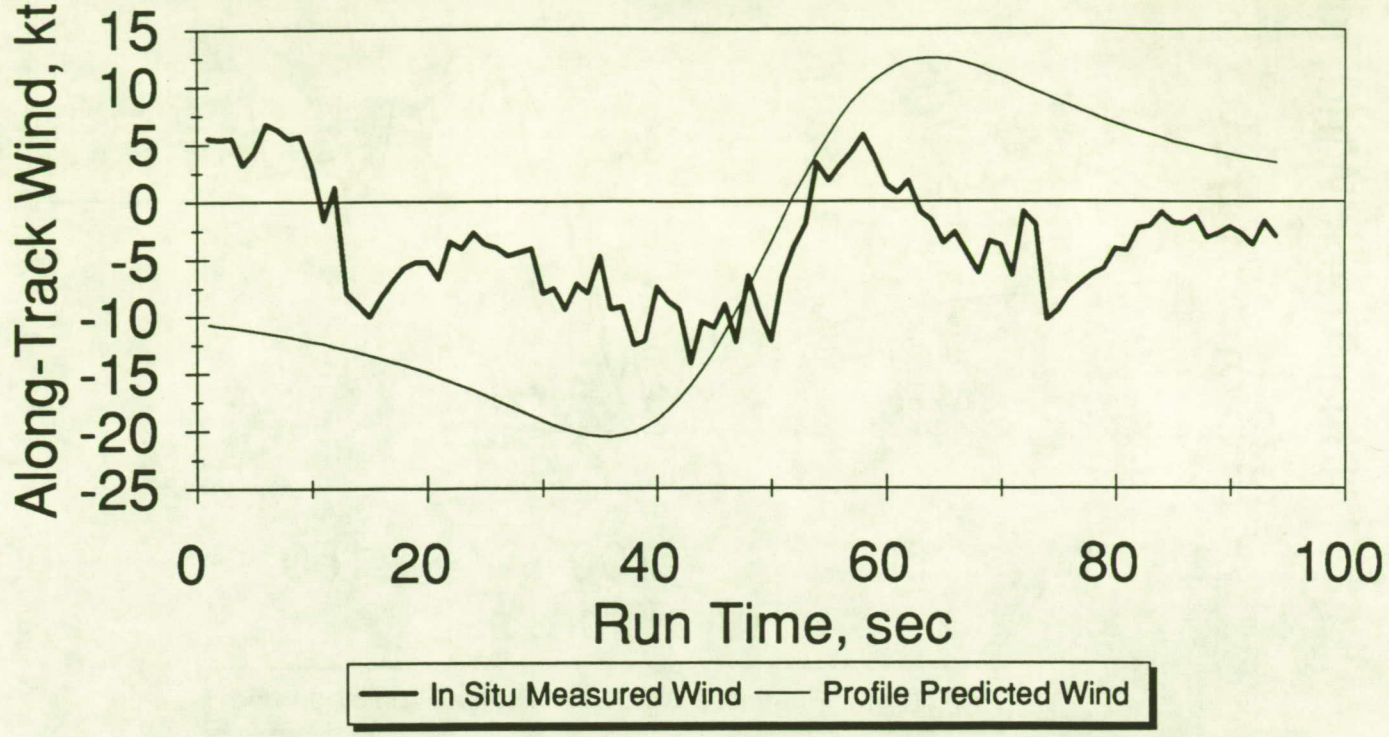

Figure 9a - Along-Track Wind Profiles for Event 81

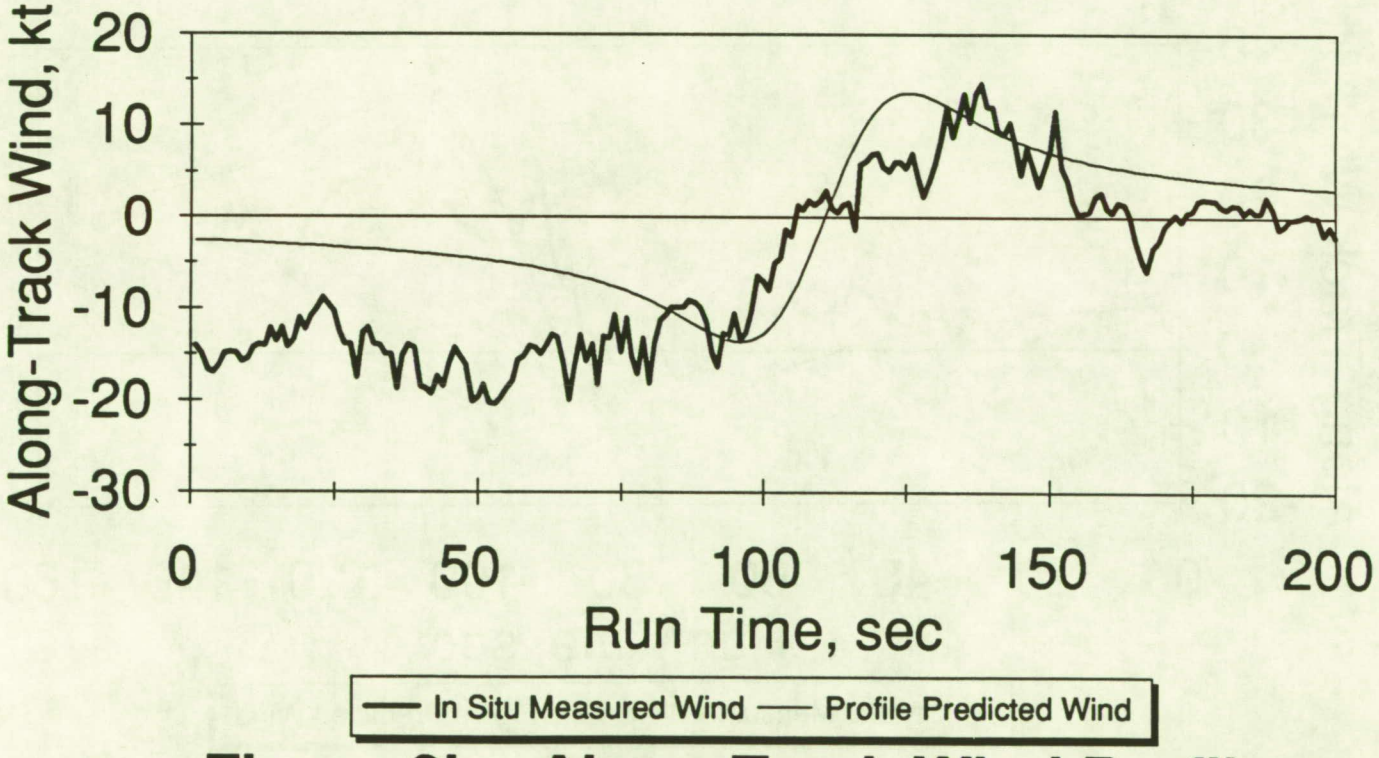

Figure 9b - Along-Track Wind Profiles for Event 134

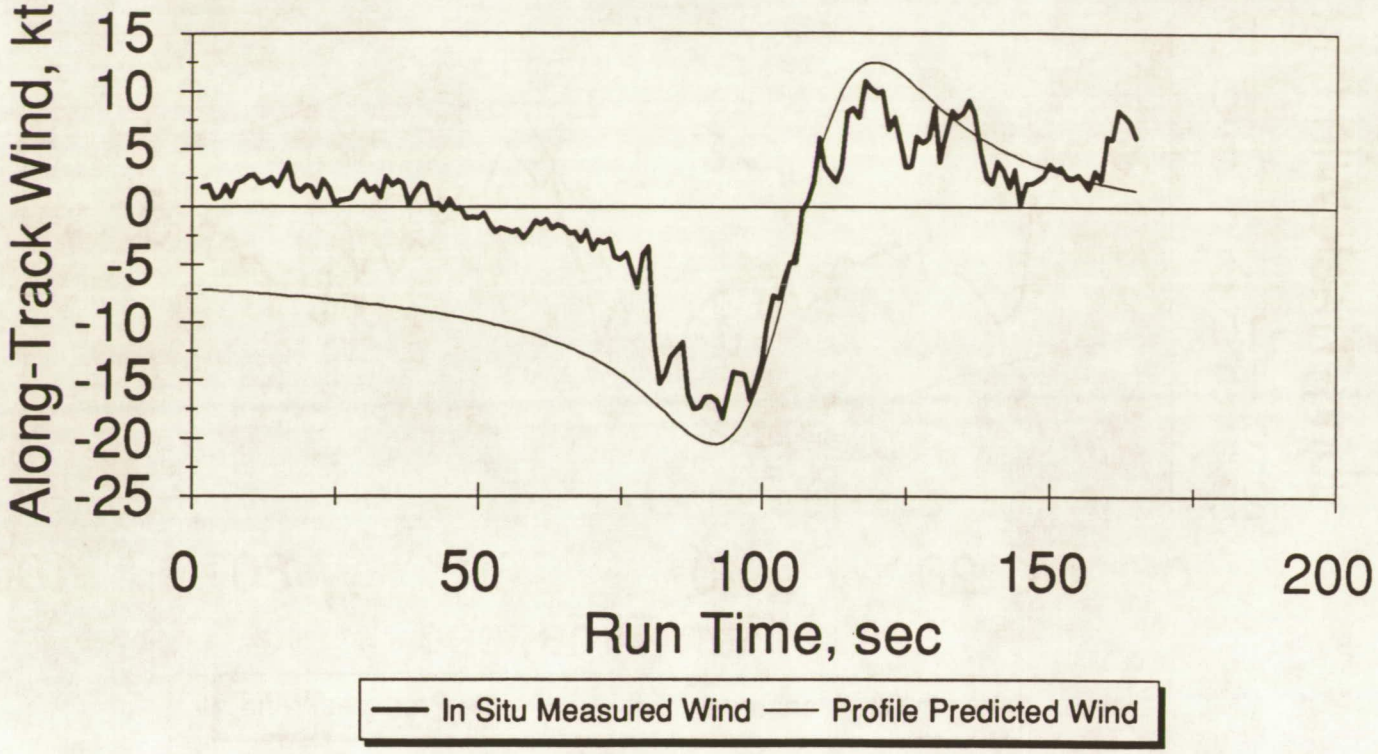

Figure 9c - Along-Track Wind Profiles for Event 142

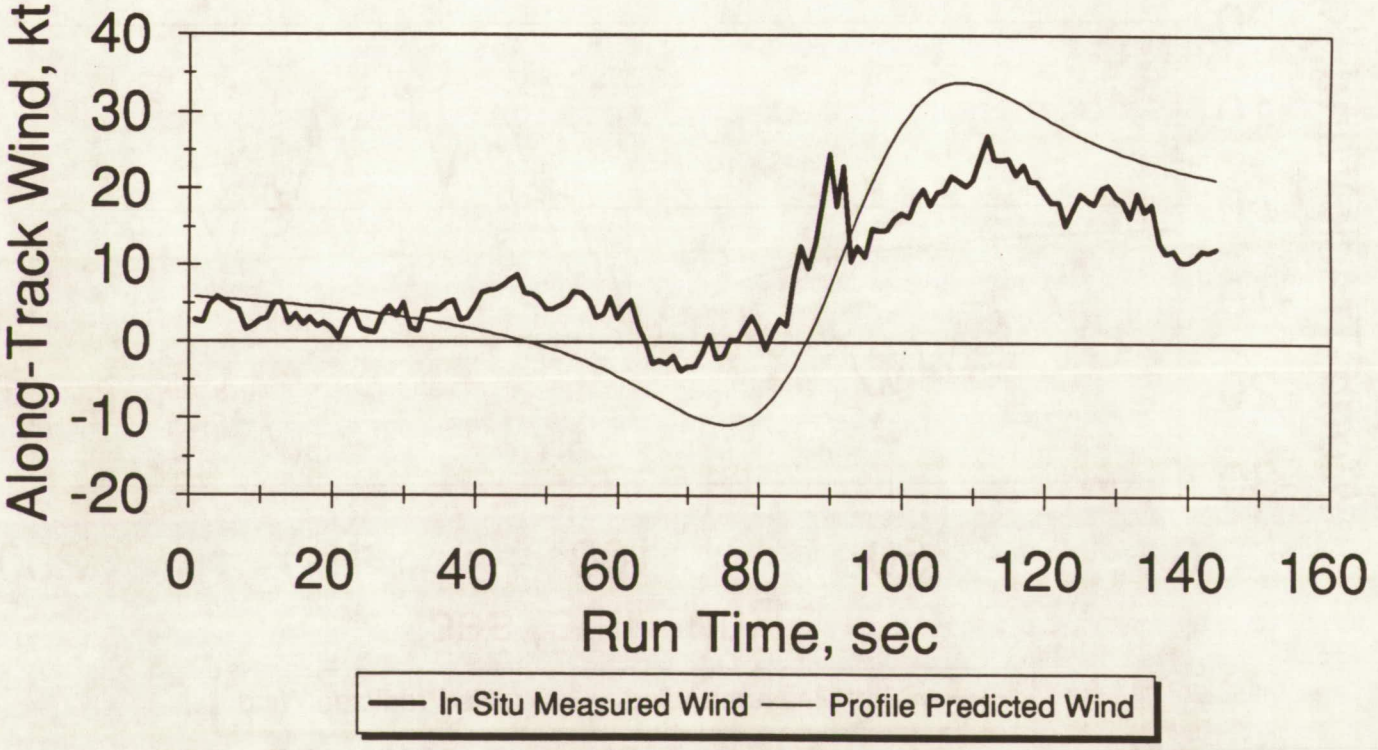

Figure 9d - Along-Track Wind Profiles for Event 143

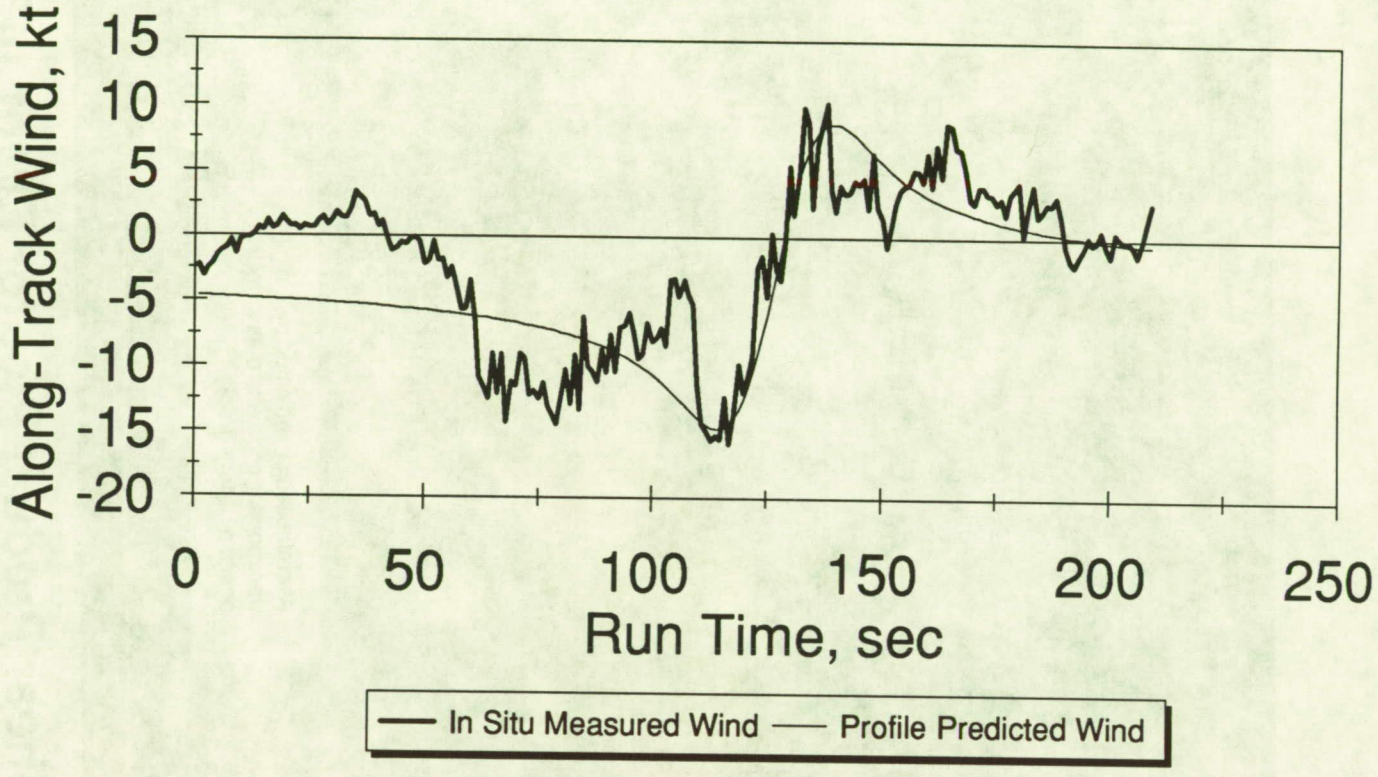

Figure 9e - Along-Track Wind Profiles for Event 144

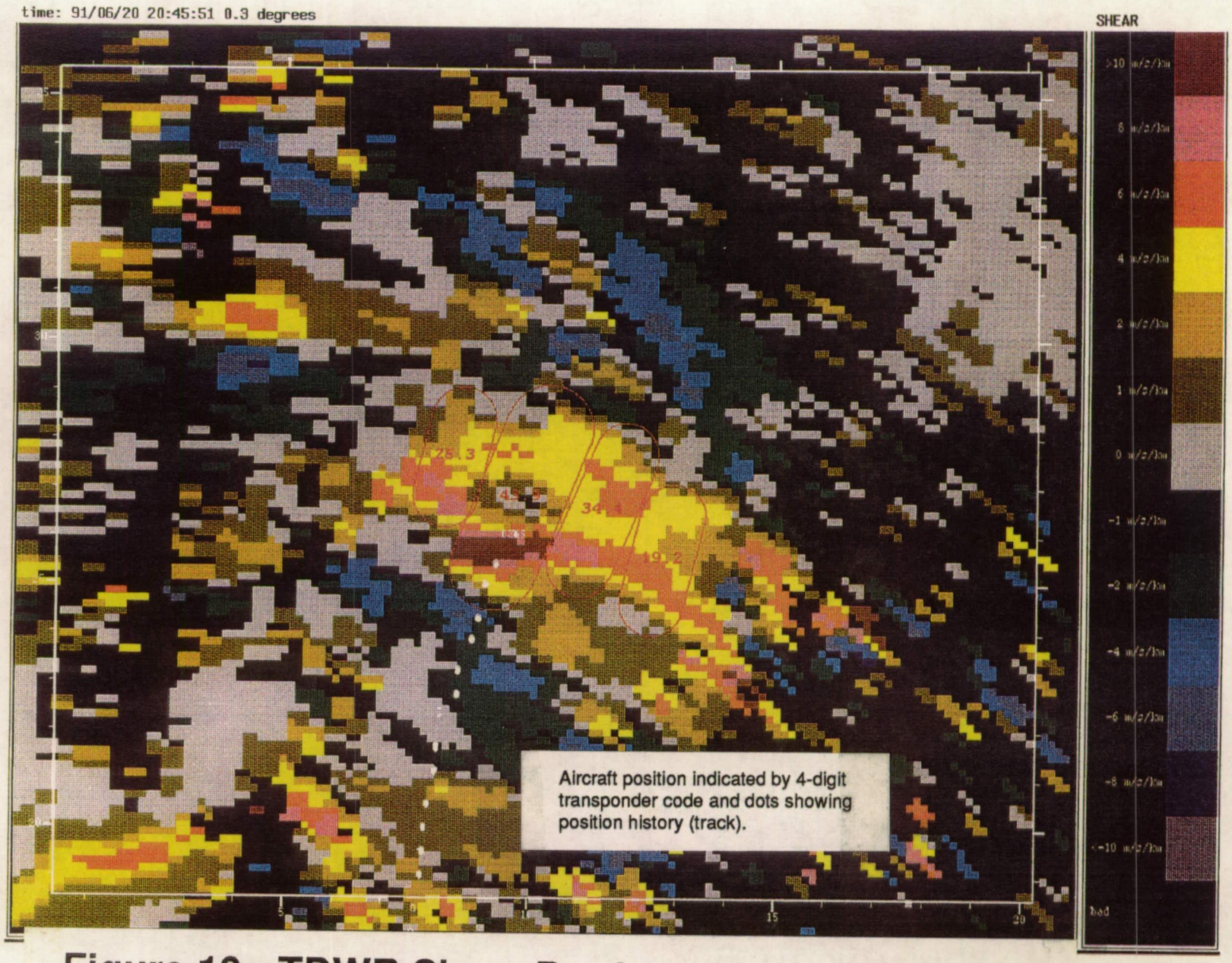

Figure 10 - TDWR Shear Product Plot for Event 143

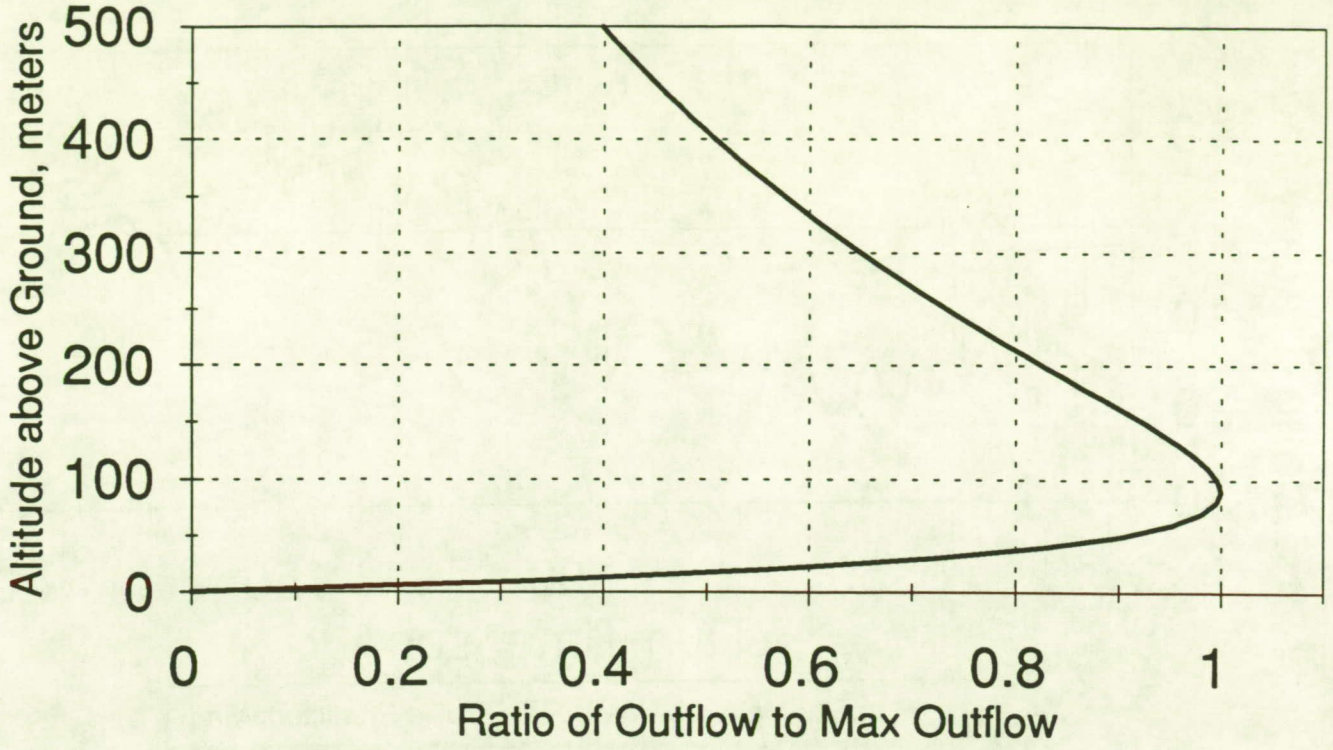

Figure 11 - Microburst Outflow Profile

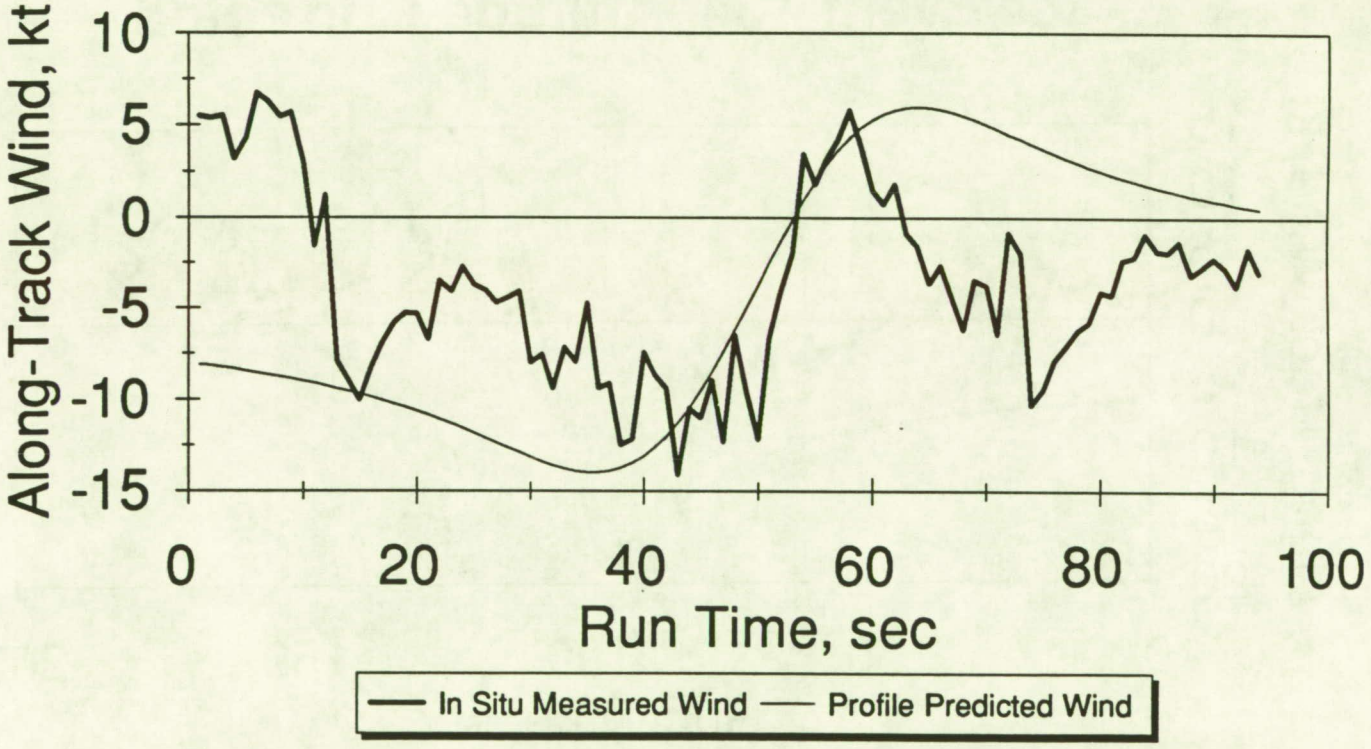

Figure 12a - Along-Track Wind Profiles for Event 81, Altitude Corrected

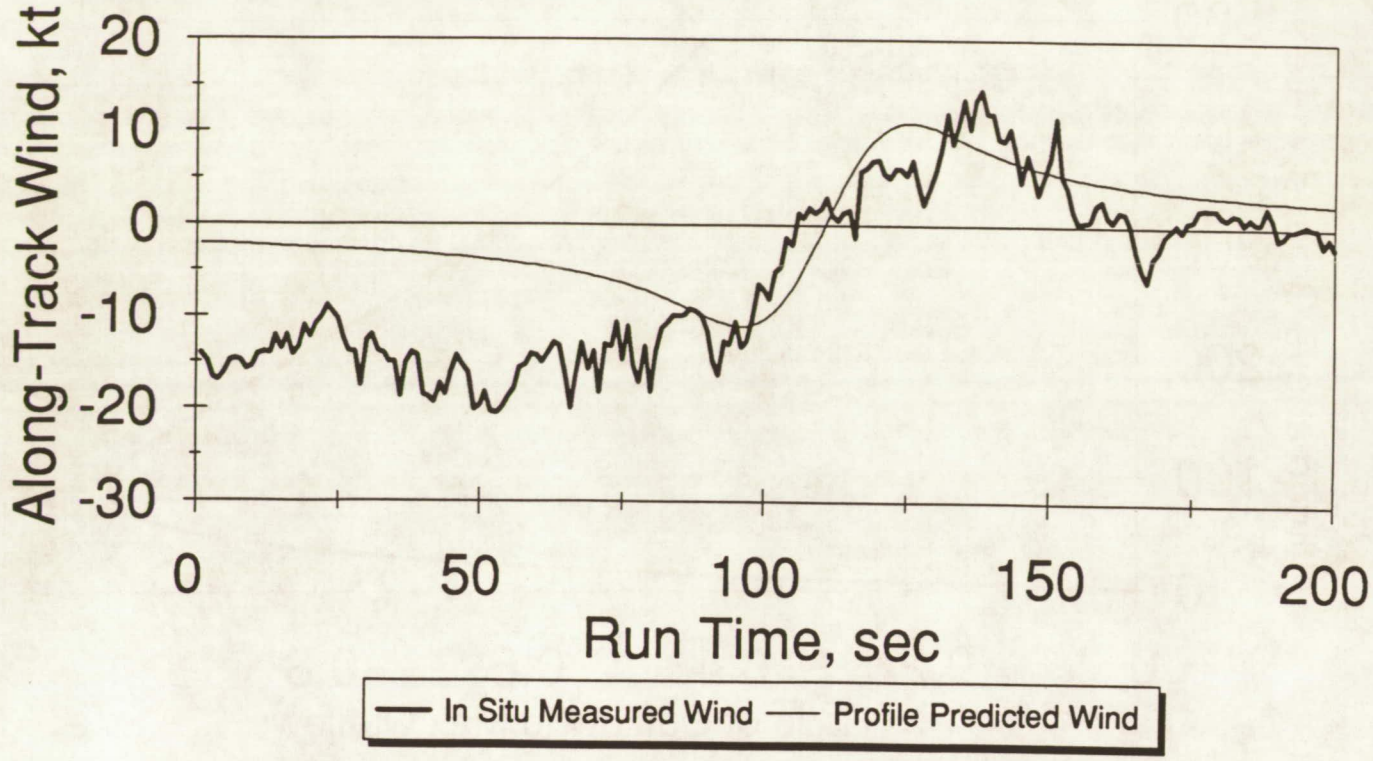

Figure 12b - Along-Track Wind Profiles for Event 134, Altitude Corrected

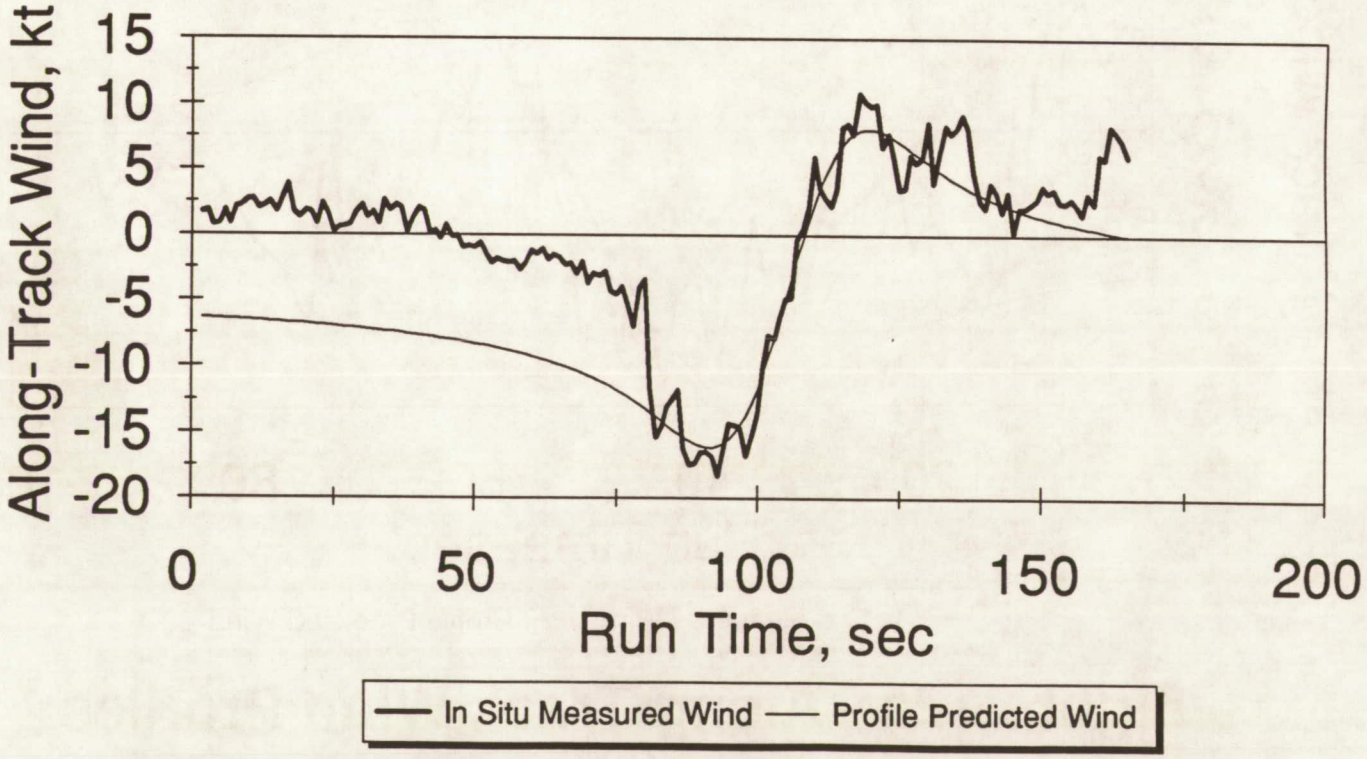

Figure 12c - Along-Track Wind Profiles for Event 142, Altitude Corrected

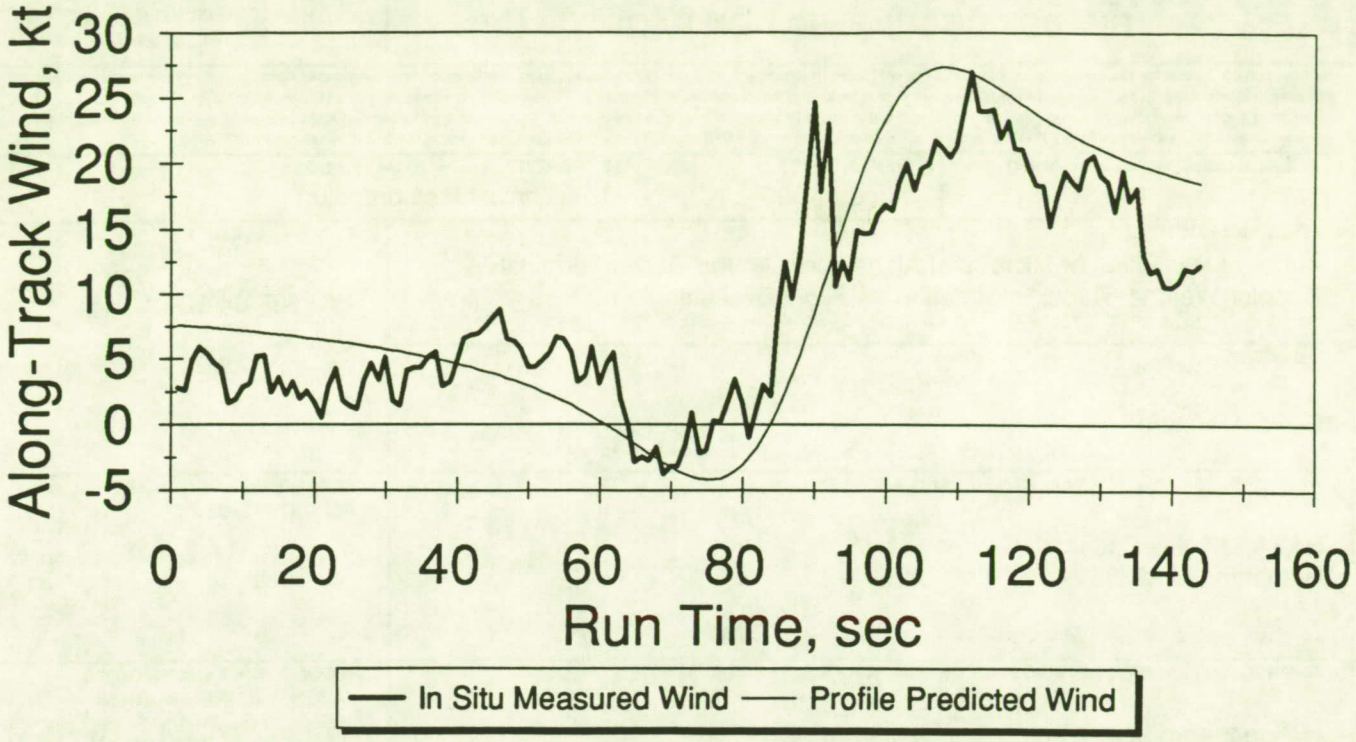

Figure 12d - Along-Track Wind Profiles for Event 143, Altitude Corrected

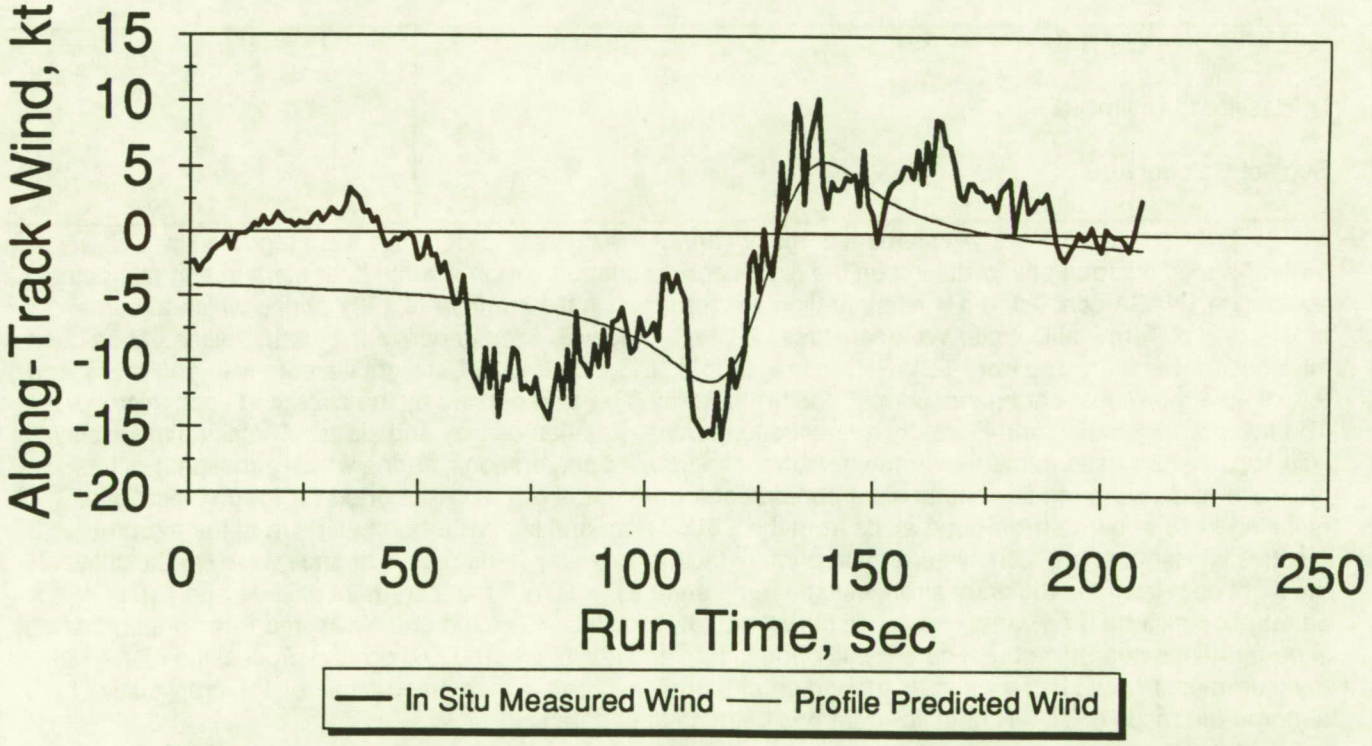

Figure 12e - Along-Track Wind Profiles for Event 144, Altitude Corrected

REPORT DOCUMENTATION PAGE

Form Approved
OMB No. 0704-0188

1. AGENCY USE ONLY *(Leave blank)*	2. REPORT DATE	3. REPORT TYPE AND DATES COVERED
	August 1993	Technical Memorandum

4. TITLE AND SUBTITLE
Airborne Derivation of Microburst Alerts from Ground-Based Terminal Doppler Weather Radar Information - A Flight Evaluation

5. FUNDING NUMBERS
WU 505-64-12-01

6. AUTHOR(S)
David A. Hinton

7. PERFORMING ORGANIZATION NAME(S) AND ADDRESS(ES)
NASA Langley Research Center
Hampton, VA 23681-0001

8. PERFORMING ORGANIZATION REPORT NUMBER

9. SPONSORING / MONITORING AGENCY NAME(S) AND ADDRESS(ES)
National Aeronautics and Space Administration
Washington, DC 20546-0001

10. SPONSORING / MONITORING AGENCY REPORT NUMBER
NASA TM-108990

11. SUPPLEMENTARY NOTES

12a. DISTRIBUTION / AVAILABILITY STATEMENT
Unclassifed - Unlimited

Subject Category 06

12b. DISTRIBUTION CODE

13. ABSTRACT *(Maximum 200 words)*

An element of the NASA/FAA windshear program is the integration of ground-based microburst information on the flight deck, to support airborne windshear alerting and microburst avoidance. NASA conducted a windshear flight test program in the summer of 1991 during which airborne processing of Terminal Doppler Weather Radar (TDWR) data was used to derive microburst alerts. Microburst information was extracted from TDWR, transmitted to a NASA Boeing 737 in flight via data link, and processed to estimate the windshear hazard level (F-factor) that would be experienced by the aircraft in each microburst. The microburst location and F-factor were used to derive a situation display and alerts. The situation display was successfully used to maneuver the aircraft for microburst penetrations, during which atmospheric "truth" measurements were made. A total of 19 penetrations were made of TDWR-reported microburst locations, resulting in 18 airborne microburst alerts from the TDWR data and two microburst alerts from the airborne reactive windshear detection system. The primary factors affecting alerting performance were spatial offset of the flight path from the region of strongest shear, differences in TDWR measurement altitude and airplane penetration altitude, and variations in microburst outflow profiles. Predicted and measured F-factors agreed well in penetrations near microburst cores. Although improvements in airborne and ground processing of the TDWR measurements would be.required to support an airborne executive-level alerting protocol, the practicality of airborne utilization of TDWR data link data has been demonstrated.

14. SUBJECT TERMS
Data Link; Windshear; Microburst;
Terminal Doppler Weather Radar; Weather Systems

15. NUMBER OF PAGES
30

16. PRICE CODE
A03

17. SECURITY CLASSIFICATION OF REPORT	18. SECURITY CLASSIFICATION OF THIS PAGE	19. SECURITY CLASSIFICATION OF ABSTRACT	20. LIMITATION OF ABSTRACT
Unclassified	Unclassified		